Wideband Spectrum Sensing for Cognitive Radios in the Presence of Correlation Between Subband Occupancy

Khalid Shamsuddin Hossain

Department of Electrical & Computer Engineering
McGill University
Montréal, Canada

November 2010

A thesis submitted to McGill University in partial fulfilment of the requirements for the degree of Master of Engineering.

2010/11/18

Abstract

Energy detection has emerged as a prime technique for wideband spectrum sensing in cognitive radio applications. Much of the present research in the area of energy detection assumes that the occupancy of any particular frequency subband is independent of the occupancy of other subbands. However, in practice, subband occupancy is likely to be correlated, for instance, due to the use of wideband transmission signals by existing users, such as broadcast television. Incorporation of the prior knowledge of such correlation into the design of channel occupancy detectors can substantially enhance the wideband sensing performance.

In this thesis, we focus on the wideband spectrum sensing task for cognitive radios in the presence of correlation between the occupancies of frequency subbands. First, we formulate the maximum *a posteriori* (MAP) estimator of channel occupancy based on measurements from multiple frequency subbands. Since the complexity of the MAP estimator grows exponentially with the number of subbands, we study an alternative detector, in which the energy measurements from all the subbands are linearly combined according to a minimum mean-square error (MMSE) criterion to form a sufficient statistic for binary hypothesis-testing in each subband. Furthermore, we incorporate this optimum linear energy combiner into single-user and collaborative multiband joint detection schemes that maximize the opportunistic spectrum usage while limiting the total probabilistic interference introduced to existing users.

Through analysis and numerical experiments, we demonstrate that the proposed frequency-coupled detector significantly outperforms the conventional decoupled one in both single-user and collaborative detection schemes.

Sommaire

La mesure d'énergie est aujourd'hui la technique la plus importante pour la détection du spectre large-bande dans les applications de radios cognitives. La plus grande partie de la recherche dans ce domaine de nos jours assume que le contenu d'une sous-bande de fréquence quelconque est indépendant de ceux des autres sous-bandes. Cependant, d'un point de vue pratique, les occupations des différentes sous-bandes sont probablement corrélées, par exemple, à cause de l'utilisation de la transmission de signaux large-bande par des utilisateurs existants telle que la transmission de la télévision hertzienne. L'intégration d'une telle corrélation dans les modèles des détecteurs des occupations des canaux de transmission peut largement améliorer la performance de la détection large-bande.

Dans cette thèse, nous nous concentrons sur la détection du spectre large-bande dans les radios cognitives en présence de corrélations entre les occupations des sous-bandes. Dans un premier temps, nous formulons l'estimateur maximum *a posteriori* (MAP) de l'occupation du canal à partir de mesures faites sur plusieurs sous-bandes. Compte tenu du fait qu'un tel estimateur devient exponentiellement plus complexe avec le nombre de sous-bandes, nous étudions un nouveau détecteur. Dans ce dernier, les mesures d'énergies des différentes sous-bandes sont linéairement combinées avec comme critère l'erreur quadratique moyenne minimale (EQMM) afin d'obtenir une statistique suffisante pour un test d'hypothèse binaire dans chaque sous-bande. Un tel détecteur linéaire est en outre incorporé dans des systèmes de détection à un ou plusieurs utilisateurs. Ces systèmes maximisent l'utilisation du spectre tout en limitant la probabilité totale de l'interférence causée aux utilisateurs existants.

À l'aide d'analyses approfondies et d'expériences numériques, nous démontrons que le détecteur avec fréquences couplées que nous proposons est largement supérieur aux détecteurs avec fréquences découplées habituels, que ce soit dans les systèmes de détection d'un unique utilisateur ou ceux de plusieurs utilisateurs.

Acknowledgments

I would like to thank my supervisor, Prof. Benoît Champagne, for his insightful guidance and motivation at every step of my graduate studies. I am also grateful to Prof. Champagne for his financial support through research contracts with InterDigital Canada Ltée., and grants from NSERC Canada. I would also like to thank the Faculty of Engineering at McGill University for the Principal's Graduate Fellowship award which proved very helpful in my pursuit of the master's degree.

Many thanks are due to my friends, and to my colleagues at the Telecommunications and Signal Processing Laboratories: Reza Abdolee, Neda Ehtiati, Gabriel Vlad Feyer, Bo Gao, Yong Jing Kim, Mohamed Konate, Eric Ploudre, Siavash Rahimi, Fang Shang, Yunhao Tian, Chao-Chen Tu, Arash Vakili, Judith Wang and Chao Zhao. I would particularly like to thank Mohamed Konate for providing the French translation of the abstract. Dr. Rocco Di Girolamo, Dr. Afshin Haghighat, and Dr. Benoît Pelletier, from InterDigital Canada Ltée., provided invaluable feedback regarding various aspects of my research, for which I am grateful to them. I would also like to thank my friend, Nahleen Zahra, for her continued support and motivation.

Finally, I would like to express my thanks to my family members for their support through all my endeavours. In particular, I am very grateful to my mother, Nadira Sultana, and my father, Mohammed Shahabuddin, for their unconditional love and encouragement, without which none of my life's accomplishments would have been possible.

Contents

1 Introduction **1**

1.1 Wideband Spectrum Sensing for Cognitive Radios 1

1.2 Objective and Contributions of the Thesis 4

1.3 Organization of the Thesis 5

2 An Overview of Spectrum Sensing Techniques **7**

2.1 Feature Detection 7

2.1.1 Use of Wavelet Transform to Detect Discontinuity in Spectrum Utilization 8

2.1.2 Use of Cyclostationarity to Detect and Classify EU Signals 10

2.1.3 Matched Filtering (Coherent) Detection 11

2.2 Energy Detection 13

2.2.1 Single-User Multiband Joint Detection 14

2.2.2 Collaborative Multiband Joint Detection 20

2.3 Final Remark 24

3 Optimum Detectors of Multiband Channel Occupancy **25**

3.1 Model for Multiband Channel Occupany 25

3.2 Bayesian Estimation of Channel Occupancy Vector 28

3.2.1 Estimation of Channel Occupancy for $K = 2$ Case 29

3.2.2 Estimation of Channel Occupancy for Uncorrelated Case 30

3.3 Optimum Linear Energy Combiner (OLEC) Detector 31

3.3.1 Lower Dimensionality Energy Combiners 34

3.3.2 Performance of the OLEC Detector 35

4 Multiband Joint Detection with the Optimum Linear Energy Combiner 37
4.1 Single-User Multiband Joint Detection 38
4.2 Collaborative Multiband Joint Detection 42
4.2.1 Optimum Linear Energy Combiner for Collaborative Detection 43
4.2.2 Performance of OLEC-based Collaborative Detection 46
4.2.3 Spatial-Spectral Joint Detection Using the OLEC 47

5 Numerical Results 51
5.1 Simulations for OLEC Performance 52
5.2 Results for Multiband Joint Detection Using the OLEC 55
5.2.1 Results for Single-User Detection 56
5.2.2 Results for Collaborative Detection 58

6 Conclusion 61
6.1 Thesis Summary 61
6.2 Future Research Directions 63

A Derivation of OLEC Weights 65

B Derivation of Moments of $\boldsymbol{Y}$ 66
B.1 Derivation of $E[\boldsymbol{Y}]$ 66
B.2 Derivation of $E[\tilde{B}_k\tilde{\boldsymbol{Y}}]$ 67
B.3 Derivation of $E[\tilde{\boldsymbol{Y}}\tilde{\boldsymbol{Y}}^T]$ 68

Bibliography 71

List of Figures

3.1 Decision regions of the MAP estimator for $K = 2$ 29
3.2 Single block of the optimum linear energy combiner (only the detector for the k-th subband is shown) 33

5.1 $P_m^{(k)}$ versus $P_f^{(k)}$ for $\rho = 0.6$ ($k = 2$, $p = 0.20$) 53
5.2 $P_m^{(k)}$ versus $P_f^{(k)}$ for $\rho = 0.7$ ($k = 2$, $p = 0.15$) 54
5.3 $P_m^{(k)}$ versus θ for $P_f^{(k)} = 0.05$ ($k = 2$) 55
5.4 The maximum aggregate opportunistic throughput of the SU against the constraint on the aggregate interference to the EU when $\rho = 0.7$ ($p = 0.15$) 57
5.5 The minimum aggregate interference to the EU against the constraint on the aggregate opportunistic throughput of the SU when $\rho = 0.7$ ($p = 0.15$) 58
5.6 The maximum aggregate opportunistic throughput of the SUs against the constraint on the aggregate interference to the EU when $\rho = 0.7$ ($p = 0.15$) 59
5.7 The minimum aggregate interference to the EU against the constraint on the aggregate opportunistic throughput of the SUs when $\rho = 0.7$ ($p = 0.15$) 60

List of Tables

5.1 Optimum Weight Vector for OLEC Detector 53
5.2 Optimum Weight Values for Reduced Dimensionality Detector 53
5.3 Parameters Used in the Single-User Multiband Joint Detection Experiment 57
5.4 Parameters Used in the Collaborative Multiband Joint Detection Experiment . . . 59

Notation

X^T	Transpose of a matrix X
X^*	Complex conjugate of a matrix
X^H	Hermitian transpose of a matrix
X^{-1}	Inverse of a (square) matrix
$\|x\|$	Absolute value of a scalar or a complex number
$\|\|\boldsymbol{x}\|\|_2$	Euclidean norm of vector $\boldsymbol{x}$: $\|\|\boldsymbol{x}\|\|_2 = \sqrt{\boldsymbol{x}^H\boldsymbol{x}}$
$\mathrm{diag}\{\boldsymbol{x}\}$	Diagonal matrix with the entries of vector $\boldsymbol{x}$ on its main diagonal
$E[\cdot]$	Expected value of a random variable
Var$[\cdot]$	Variance of a random variable
$\triangleq$	Defined to be
$\equiv$	Equivalent to (notational)
$\circledast$	Linear convolution operator
$\ln(\cdot)$	Natural logarithm (to base e)
I_N	$N \times N$ identity matrix
$\mathbf{1}$	Column vector whose elements are all 1
$Q(\cdot)$	Tail probability of a standard normal random variable: $Q(x) \triangleq \frac{1}{\sqrt{2\pi}} \int_x^\infty e^{-t^2/2}\, dt$
δ_{ij}	Kronecker's delta function: $\delta_{ij} = \begin{cases} 1 & \text{if } i = j \\ 0 & \text{otherwise} \end{cases}$
$\mathcal{N}(\mu, \sigma^2)$	Real-valued Gaussian distribution with mean μ and variance σ^2
$\mathcal{CN}(\mu, \sigma^2)$	Complex circular symmetric Gaussian distribution with mean μ and variance σ^2
$\mathbb{N}$	The set of all non-negative integers: $\{0, 1, 2, \ldots\}$

List of Acronyms

CR	Cognitive Radio
DFT	Discrete Fourier Transform
DTFT	Discrete-Time Fourier Transform
EU	Existing User
FFT	Fast Fourier Transform
MAP	Maximum A Posteriori
MSE	Mean Square Error
OLEC	Optimum Linear Energy Combiner
PDF	Probability Density Function
PMF	Probability Mass Function
PSD	Power Spectral Density
PU	Primary User
ROC	Receiver Operating Characteristic
SCF	Spectral Correlation Function
SU	Secondary User

Chapter 1

Introduction

In this chapter, we introduce the topic of spectrum sensing in the context of cognitive radios and briefly present some of the prominent techniques conventionally used in sensing tasks. This is followed by the objective and a brief summary of the contributions of this thesis. Finally, the organization of the thesis is outlined.

1.1 Wideband Spectrum Sensing for Cognitive Radios

Historically, wireless communication systems, such as broadcast radio/television and mobile phones, have been allocated frequency bands for dedicated usage. That is, a particular type of wireless device must use a pre-allocated frequency band at a particular location and time. In recent years, an ever-increasing demand for multimedia applications has fuelled the proliferation of high data-rate wireless devices, resulting in a shortage of frequency bands available for licensing. However, studies by the Federal Communications Commission (FCC) show that, in certain locations, the average spectrum occupancy is only 5.2% with a maximum occupancy of 13.1% at any point in time [1],[2]. Therefore, the apparent lack of radio resources can be worked around

if the empty frequency bands can be detected and opportunistically used through a suitable mechanism. In other words, despite the lack of spectrum availability for licensing, more wireless devices may be accomodated if a dynamic spectrum access model is deployed to complement the static allocation model currently in use.

In this context, a momentarily unused portion of the frequency spectrum is called a *spectrum hole* and has been defined in [3] as *a band of frequencies assigned to a primary user, but, which, at a particular time and specific geographic location, is not being utilized by that user*. Spectrum sensing is the process of detecting such spectrum holes. Here, the *primary user* (PU) is the wireless system to which the band of frequency in question has been licensed. In many instances, this could be the user of a legacy technology, such as broadcast television.

Cognitive radios (CR) have emerged as a promising technology for incorporation of a dynamic spectrum access model. [4] defines cognitive radio as *a radio or system that senses its operational electromagnetic environment and can dynamically and autonomously adjust its radio operating parameters to modify system operation, such as maximize throughput, mitigate interference, facilitate interoperability, access secondary markets*. Thus, CRs must have the capability to detect and opportunistically use any available spectrum holes. In this scenario, one refers to the CR in question as a *secondary user* (SU). Spectrum sensing based on the observation of wideband radio signals has gained further importance as CR is an integral component of the IEEE 802.22 wireless standard [5]. In practice, spectrum sensing must be reasonably fast and accurate so as to maximize the opportunistic throughput without adding unacceptable level of interference to the existing users (EU), including the PUs and other SUs.

Traditionally, several different approaches have been used to perform sensing tasks. Some of the methods popularly considered for CR applications are matched filtering, feature detection and energy detection. Matched filtering is a well-known technique used to demodulate communication signals [6]. It relies on the convolution of a received signal with a sample test signal to

measure the cross-correlation. As shown in [7], this technique can also be exploited to perform sensing tasks. However, a strong dependence on time synchronization and on the knowledge of the primary signal makes the use of matched filtering impractical for detection problems.

The use of special signal features to detect and classify PU signals has been studied in recent years. For instance, cyclostationarity features are used to detect and classify primarily signals in [8]. Here, the periodic nature of the modulating signals is exploited through the computation of cyclic autocorrelation. In [9], the wavelet transform is used to locate discontinuities in the wideband power spectral density (PSD) in order to detect the unused portions of the spectrum. Feature-based detection typically results in elaborate and complex detector structures that lack customizability for particular applications.

Many studies, such as [10] and [11], advocate the use of energy detection for spectrum sensing since it can meet the basic requirements of CR systems while offering flexibility and robustness in implementation. Energy detection schemes compute the energy of the received signal and then carry out hypothesis tests to decide the occupancy state of the frequency band(s) in question. Such schemes can be used in both narrowband and wideband paradigms. Wideband detection, for example, may be performed by dividing the broad frequency band into smaller component subbands and carrying out narrowband detection in these individual subbands independently.

Multiband energy detection is of particular interest as it can significantly improve the overall achievable throughput. For example, [12] considers a scheme in which the cost of interfering with each of the EUs and the Shannon theoretic capacity for each subband are used to define global measures for *aggregate interference* and *aggregate opportunistic throughput* respectively. Consequently, the goal of the detection task is to maximize the opportunistic throughput aggregated over all the subbands while keeping the aggregate interference under a critical value, or, conversely, to minimize the aggregate interference across all the subbands while satisfying a lower bound on acceptable aggregate opportunistic throughput. This scheme is discussed in further

detail in Section 2.2.

Furthermore, to overcome blockage effects in wireless transmissions, e.g., multipath fading or shadowing, spectrum sensing may also be carried out by a cluster of collaborating CRs. This approach, known as distributed or collaborative sensing, is generally expected to outperform single-user detection and is considered in, e.g., [2],[13], and [14]. While energy detection schemes have gained popularity, the schemes currently being considered rely on specific assumptions about the channel occupancy model that constrict the applicability of the resulting detectors.

1.2 Objective and Contributions of the Thesis

The current literature on wideband energy detection for spectrum sensing focuses on a decoupled multiband processing structure in which energy detection in any given subband is based on a sufficient statistic computed from observed data in that particular subband only, i.e., independently of other subbands' data. Even sophisticated multiband detection schemes such as [12], while jointly optimizing the set of detection thresholds used in the individual subbands from a wideband perspective, make use of this decoupled structure. Although such a structure is indeed optimal under the assumption that the occupancies of the frequency subbands are independent of each other, this assumption is generally not true, especially in the presence of wideband PU/EU signals, e.g., broadcast television or WLAN systems [15]. As a result, more recently, the topic of spectrum sensing in the presence of correlated subband occupancy has been gaining much attention. For example, [16] considers an autoregressive model to track the strengths of EU signals along frequencies and delimit their spectral support. A sub-optimal binary detector that sums the energy over the identified spectral band is then employed to perform spectrum sensing.

The objective of this thesis is to consider the spectrum sensing problem in a multiband framework where *a priori* knowledge about the correlation across subband occupancies is exploited

to enhance the sensing performance. To achieve this, we introduce a vector of binary random variables to model the multiple subband occupancies. By considering a Bayesian framework, we formulate the maximum *a posteriori* (MAP) estimator of the wideband channel occupancy vector based on the measurements from multiple subbands. The MAP estimator reduces to a decoupled structure when the subband occupancies are independent of each other, but, in the general case, its complexity grows exponentially with the number of subbands. An alternative structure is therefore proposed where the energy measurements from multiple subbands are linearly combined, with weights derived from a minimum mean-square error (MMSE) criterion, to form a sufficient statistic for binary detection in each subband. Through both analysis and numerical simulations, it is demonstrated that the proposed optimum linear energy combiner (OLEC) can significantly outperform (in the Neyman-Pearson sense) the traditional decoupled detector currently being considered.

Additionally, the performance of the OLEC detector when used in conjunction with existing spectrum sensing schemes is studied in this thesis. In particular, the OLEC detector is tested within the multiband joint detection frameworks presented in [12]. Instead of using decoupled hypothesis tests on the energy measurements from individual subbands, we use the test statistics obtained from linearly combining energy measurements from multiple subbands. Through numerical analysis, we show that the OLEC detector offers significant performance gains when incorporated into both single-user and collaborative joint detection frameworks.

1.3 Organization of the Thesis

This thesis is structured as follows. In Chapter 2, an overview of spectrum sensing methodologies is presented in the form of a survey of selected recent literature in this area. In Chapter 3, a suitable system model for multiband energy detection is presented, followed by the development

of the optimum Bayesian detector and the optimum linear energy combiner (OLEC), along with an analysis of the latter's performance. Chapter 4 shows how the OLEC detector may be used in the context of the single-user multiband joint detection and the spatial-spectral joint detection structures developed in [12] in order to enhance the detection performance of such sophisticated schemes. Chapter 5 presents numerical results to corroborate the analytical developments in Chapters 3 and 4. Finally, in Chapter 6, the thesis is summarized and conclusions are drawn.

Chapter 2

An Overview of Spectrum Sensing Techniques

As discussed in Section 1.1, traditionally, a few different techniques have been employed in spectrum sensing tasks. Of these, feature detection, matched filtering, and energy detection have been most prominently studied for cognitive radio applications. In this section, each of these is briefly outlined. In particular, the work in [7] is discussed in detail as an example of an elaborate scheme for multiband joint detection in both single-user and collaborative frameworks. It will serve as a basis for the development of the new material presented in Chapter 4.

2.1 Feature Detection

Presently, a few different feature detection techniques are being studied. Three of the main schemes are discussed below:

- Wavelet transform to locate discontinuities in the wideband power spectral density;
- Exploiting cyclostationary features to detect and classify primary signals; and

- Matched filtering to coherently detect the presence of primary signals.

2.1.1 Use of Wavelet Transform to Detect Discontinuity in Spectrum Utilization

The wavelet transform is discussed in detail in [9] and [17]. Its use has been proposed in the context of spectrum sensing to detect discontinuities in the frequency spectrum, and then estimate the power spectral density (PSD) in each frequency subband. The bandwidth of interest is assumed to consist of K adjacent subbands in the frequency range $B = [f_0, f_K]$, where the PSD in the k-th subband, $B_k = [f_{k-1}, f_k]$, is smooth and almost flat, with the parameter f_k representing the subband edge frequencies. Therefore, the discontinuities in the PSD mark the edges of the subbands. Additive background white noise with power spectrum $S_v(f) = N_0/2$ is assumed to be present at all times, where f denotes the frequency variable (in Hz). If the normalized power spectral shape in the k-th band is written as:

$$S_k(f) = \begin{cases} 1 & \text{if } f \in B_k \\ 0 & \text{if } f \notin B_k \end{cases} \tag{2.1}$$

then the PSD of observed signal can be expressed as:

$$S_r(f) = \sum_{k=1}^{K} \alpha_k^2 S_k(f) + S_v(f) \tag{2.2}$$

where α_k^2 is the EU signal power density within the k-th subband, and $p_k(t)$ is a basic time-domain signal corresponding to the PSD shape (2.1). Equivalently, the time-domain representation of the observed signal is:

$$r(t) = \sum_{k=1}^{K} \alpha_k p_k(t) + v(t) \tag{2.3}$$

As a result, the problem is reduced to the estimation of the parameters N, $\{f_k\}_{k=1}^{K-1}$, and $\{\alpha_k^2\}_{k=1}^{K}$ based on an estimate of the observed signal PSD, denoted here as $\hat{S}_r(f)$.

In the frequency domain, the wavelet function is represented by $\phi_s(f) = \frac{1}{s}\phi(\frac{f}{s})$ with Fourier transform pair $\Phi_s(\tau) = \Phi(s\tau)$. Commonly used wavelet function, $\phi(f)$, includes the Gaussian function [18],[19]. The continuous wavelet transform of $\hat{S}_r(f)$ is given by:

$$W_s\{\hat{S}_r(f)\} = \hat{S}_r(f) \circledast \phi_s(f) \tag{2.4}$$

where s represents the scale factor, i.e., $s = 2^j$ with $j = \{1, 2, ..., J\}$, and $\circledast$ denotes the linear convolution integral over the frequency f.

Since the objective is to detect discontinuities in the PSD of $\hat{S}_r(f)$, the transform is carried out in the frequency domain. Discontinuities in the frequency domain are given by the extrema of the first derivative and by the zero values of the second derivative of the wavelet transform [18]. Hence, the frequency boundaries can be estimated by:

$$\hat{f}_k = \arg\max |U(f)|, \quad f \in [f_0, f_K] \tag{2.5}$$

where

$$U(f) \triangleq \prod_{j=1}^{J} W'_{s=2^j}\{\hat{S}_r(f)\} \tag{2.6}$$

is a multiscale wavelet product used to remove the noise-induced maxima that are random at different scales [9].

The PSD within the k-th band is $\hat{\beta}_k = \frac{1}{f_k - f_{k-1}} \int_{f_{k-1}}^{f_k} \hat{S}_r(f)df$. Since $\min_k \hat{\beta}_k$ represents the estimate of the noise power, the PSD of the EU signal is given by:

$$\hat{\alpha}_k^2 = \hat{\beta}_k - \min_k \hat{\beta}_k, \quad k = 1, \ldots, K \tag{2.7}$$

Although the numerical results presented in, e.g., [9], are very accurate, this method relies on the presence of sharp discontinuities in the PSD along the frequency axis. In reality, the PSD is expected to be somewhat smoother, making the use of wavelet transforms very difficult in practice.

2.1.2 Use of Cyclostationarity to Detect and Classify EU Signals

References [8], [20] and [21] present the use of cyclostationarity properties of the observed signal to detect and classify any EU signals present. A thorough treatment of the use of cyclostationarity for detection or classification tasks can be found in [22] and [23]. Typically, the EU signal is a modulated sinusoidal carrier and, hence, can be modelled as a wide-sense second-order cyclostationary process with period T_0, where $T_0 \neq 0$ represents the fundamental period of the process. Therefore, its mean and autocorrelation functions are periodic with period T_0. Let $s(n)$ denote the discrete-time representation of the EU signal. The cyclic auto-correlation function of $s(n)$ is defined as [23]:

$$R_s^{\alpha}(m) \triangleq E[s(n)s^*(n+m)e^{-2\pi\alpha n}] \tag{2.8}$$

where α represents the integer multiples of the reciprocal of the fundamental period, T_0. This function has a finite non-zero value for $\alpha = i/T_0, \forall i \in \mathbb{Z}^+$ and is equal to 0 otherwise. The spectral correlation function (SCF), denoted as $S_s^{\alpha}(e^{j\omega})$, where $\omega \in [-\pi, \pi]$ is the digital frequency corresponding to a sampling rate of F_s, is defined as the discrete-time Fourier transform (DTFT) of $R_s^{\alpha}(m)$.

The SCF of the observed moving signal $r(n)$ can be estimated using:

$$\hat{S}_r^{\alpha}(k) = \frac{1}{N}\sum_{n=1}^{N} R_L\Big(n, k + \frac{k_\alpha}{2}\Big) R_L^*\Big(n, k - \frac{k_\alpha}{2}\Big) \tag{2.9}$$

where $R_L(n,k)$ is the L-point DFT of the observed signal around the n-th sample, $k_\alpha = \alpha L/F_s$ is the index of the frequency bin corresponding to the cyclic frequency α, and N is the total number of observed samples available. Given the above estimate, the following hypothesis test can be used to detect the presence of the EU signal:

$$\sum_{k=0}^{L-1} \hat{S}_r^\alpha(k)[S_s^\alpha(k)]^* \underset{\mathcal{H}_0}{\overset{\mathcal{H}_1}{\gtrless}} \gamma \tag{2.10}$$

Here, hypotheses $\mathcal{H}_0$ and $\mathcal{H}_1$ correspond to the absence and presence of an EU respectively. Reference [8] treats the above in the continuous time and also presents ways of classifying the observed signal in terms of its period using a hidden Markov model (HMM) classifier. As is clear from (2.10), to perform these tests, *a priori* knowledge of the EU signal, especially its SCF, $S_s^\alpha(k)$, is essential. This information is generally not available in practice.

2.1.3 Matched Filtering (Coherent) Detection

In certain applications, it is possible to have *a priori* knowledge of the primary signal waveform, $s(n)$, e.g., due to known pilot signals [7]. In such cases, the CR node has complete knowledge of $s(n)$, and, given an observed signal $r(n)$, a matched filtering technique can be used to detect the presence of the EU signal using:

$$T \triangleq \sum_{n=1}^{N} r(n)s^*(n) \underset{\mathcal{H}_0}{\overset{\mathcal{H}_1}{\gtrless}} \gamma \tag{2.11}$$

where γ is a user-defined threshold parameter.

Under hypothesis $\mathcal{H}_0$, it can be shown that, for large N, the test statistic is normally distributed with zero mean and variance $Np_s\sigma_v^2$, i.e., $T \sim \mathcal{CN}(0, Np_s\sigma_v^2)$, where σ_v^2 is the noise variance and $p_s = \frac{1}{N}\sum_{n=1}^{N}|s(n)|^2$ is the average power of the EU signal. Similarly, under under $\mathcal{H}_1$, it can be

shown that $T \sim \mathcal{CN}(Np_s, Np_s\sigma_v^2)$ [7]. Consequently, the probabilities of false alarm and missed detection can be expressed respectively as:

$$P_f = P(H_1|H_0) = Q\left(\frac{\gamma}{\sigma_v\sqrt{Np_s}}\right) \tag{2.12}$$

$$P_m = P(H_0|H_1) = 1 - Q\left(\frac{\gamma - Np_s}{\sigma_v\sqrt{Np_s}}\right) \tag{2.13}$$

where $Q(.)$ represents the tail probability of a standard normal random variable defined as:

$$Q(x) \triangleq \frac{1}{\sqrt{2\pi}}\int_x^\infty e^{-t^2/2}dt \tag{2.14}$$

From (2.12) and (2.13), the number of required measurements required to attain a particular operating point (P_f, P_m) can be found to be:

$$N = \left[Q^{-1}(P_f) - Q^{-1}(1 - P_m)\right]^2 \text{SNR}^{-1} = \mathcal{O}(1/\text{SNR}) \tag{2.15}$$

where $\text{SNR} \triangleq \frac{p_s}{\sigma_v^2}$ is the signal-to-noise ratio of the EU signal, and $\mathcal{O}$ is the big order notation[1].

From wireless communications theory, it is well-known that when the transmitted signal is known, the matched filter detector is optimum [6]. However, as the SNR drops, a much larger number of samples is needed to reach a desired operating point [25]. This, in addition to a strong dependence on synchronization and prior knowledge of the EU signal, makes the matched filter detection unfeasible in most cases [26].

[1] A function $f(x)$ is $\mathcal{O}(g(x))$ if there are positive real constants c and x_0 such that $f(x) \leq cg(x)$ for all values of $x \geq x_0$ [24]

2.2 Energy Detection

The energy measured in any particular frequency band can be used as an indicator of the occupancy of that band. For example, consider the narrowband case where the SU observes the discrete-time, band-limited signal

$$\mathcal{H}_0 : r(n) = v(n) \tag{2.16}$$

$$\mathcal{H}_1 : r(n) = s(n) + v(n) \tag{2.17}$$

where $n \in \{0, 1, \ldots, N-1\}$ is the time index, $s(n)$ is the EU signal and $v(n)$ is modelled as a complex Gaussian white noise sequence, i.e., $v(n) \sim \mathcal{CN}(0, \sigma_v^2)$. Based on the observation of $\left\{r(n)\right\}_{n=0}^{N-1}$, the optimum detector of the EU signal (in the Neyman-Pearson sense) can be shown to be [27]:

$$y \triangleq \sum_{n=0}^{N-1} |r(n)|^2 \underset{\mathcal{H}_0}{\overset{\mathcal{H}_1}{\gtrless}} \gamma \tag{2.18}$$

In this case, [7] shows that the number of samples required to attain an operating point (P_f, P_m) is given by:

$$N = \left[Q^{-1}(P_f) - Q^{-1}(1 - P_m)\,(1 + \text{SNR})\right]^2 \text{SNR}^{-2} \tag{2.19}$$

where the EU signal parameters, SNR and p_s, are as defined previously. When SNR $\gg 1$, (2.19) dictates that $\mathcal{O}(1/\text{SNR})$ samples are needed for a given operating point (P_f, P_m), while, in low SNR regions, where SNR $\ll 1$, $\mathcal{O}(1/\text{SNR}^2)$ samples are needed. Hence, the energy detector can produce fast results (i.e., using fewer samples) in high SNR conditions, but, in low SNR scenarios, the speed of detection deteriorates. However, because of their low cost, implementational simplicity, and flexibility (only a minimum amount of prior information about the EU signal is needed), energy-based detection schemes are often favoured in literature, e.g., in

[1], [10], [13] and [16].

The energy detector can also be applied to wideband detection scenarios. Furthermore, in order to overcome the negative impacts of multipath fading and shadowing on detection performance, energy detectors can be incorporated into multi-user collaborative schemes. For example, [12] considers both single-user and multi-user collaborative detection for wideband applications. For illustrative purposes, the findings of this particular paper are summarized below; they will serve as a basis in the developments presented in Chapter 4.

2.2.1 Single-User Multiband Joint Detection

Let $r(n)$ denote the down-converted and uniformly sampled wideband signal observed by the SU (i.e., CR detector):

$$r(n) = \sum_{l=0}^{L-1} h(l)s(n-l) + v(n) \tag{2.20}$$

where $s(n)$ is the EU signal, $h(n)$ is the impulse response of the wireless channel between the EU and the SU (assumed to be time-invariant), L is the length of $h(n)$ and $v(n)$ is an additive noise term.

We consider a frequency-domain detector structure in which a K-point discrete Fourier Transform (DFT)[2] is used to decompose successive frames of $r(n)$ into narrowband discrete frequency components, i.e.:

$$R_k(m) = \sum_{n=0}^{K-1} r(mK+n)e^{-j2\pi nk/K}, \quad k = 0, 1, ..., K-1 \tag{2.21}$$

where k is the frequency and $m \in \{0, 1, \ldots, M-1\}$ is the frame index. In a similar fashion, we let H_k, $S_k(m)$ and $V_k(m)$ denote the k-th DFT coefficients of $h(n)$, $s(mK+n)$ and $v(mK+n)$,

[2] In an actual implementation, the fast Fourier transform (FFT) algorithm is used to compute the DFT frequency samples more efficiently [28].

respectively. Under the assumption of a large time-bandwidth product ($K > L$), the convolution in (2.20) can be approximated by the product of the corresponding DFT coefficients, that is:

$$\begin{aligned} \mathcal{H}_{0,k} &: R_k(m) = V_k(m) \\ \mathcal{H}_{1,k} &: R_k(m) = H_k S_k(m) + V_k(m) \end{aligned} \tag{2.22}$$

Under hypothesis $\mathcal{H}_{0,k}$, the k-th frequency bin or subband is unoccupied, while, under $\mathcal{H}_{1,k}$, the k-th subband is occupied. The EU signal and noise samples, $\{S_k(m)\}$ and $\{V_k(m)\}$ respectively, are modelled as independent random processes. Samples from each process are assumed to be independent across frequency and frame indices and to obey a zero-mean complex circular symmetric Gaussian distribution. We set $E[|S_k(m)|^2] = 1$, while the noise variance $E[|V_k(m)|^2] = \sigma_v^2$ and the channel squared magnitude response, $G_k \triangleq |H_k|^2$, are assumed to be known from *a priori* estimation.

In [12], detection is performed using the following decision rule:

$$Y_k \triangleq \sum_{m=0}^{M-1} |R_k(m)|^2 \underset{\mathcal{H}_{0,k}}{\overset{\mathcal{H}_{1,k}}{\gtrless}} \gamma_k \tag{2.23}$$

where γ_k is the detection threshold used in the k-th subband. The central limit theorem dictates that, for a large enough M, the random variables $\{Y_k\}_{k=0}^{K-1}$ are approximately normally distributed with mean:

$$E[Y_k] = \begin{cases} M\sigma_v^2, & \mathcal{H}_{0,k} \\ M(\sigma_v^2 + |H_k|^2), & \mathcal{H}_{1,k} \end{cases} \tag{2.24}$$

and variance[3]:

$$\mathit{Var}[Y_k] = \begin{cases} M\sigma_v^4, & \mathcal{H}_{0,k} \\ M(\sigma_v^2 + |H_k|^2)^2 & \mathcal{H}_{1,k} \end{cases} \tag{2.25}$$

It follows that the probabilities of false alarm and detection associated with (2.23) can be respectively expressed as:

$$\begin{aligned} P_f^{(k)}(\gamma_k) &= Pr(Y_k > \gamma_k | \mathcal{H}_{0,k}) \\ &= Q\left(\frac{\gamma_k - M\sigma_v^2}{\sigma_v^2\sqrt{M}}\right) \end{aligned} \tag{2.26}$$

$$\begin{aligned} P_d^{(k)}(\gamma_k) &= Pr(Y_k > \gamma_k | \mathcal{H}_{1,k}) \\ &= Q\left(\frac{\gamma_k - M(\sigma_v^2 + |H_k|^2)}{(\sigma_v^2 + |H_k|^2)\sqrt{M}}\right) \end{aligned} \tag{2.27}$$

In the wideband case, the detection thresholds, the probabilities of false alarm and the probabilities of missed detection for the K subbands can be represented compactly using the vector notation:

$$\boldsymbol{\gamma} \equiv [\gamma_0, \gamma_1, \ldots, \gamma_{K-1}]^T \tag{2.28}$$

$$\boldsymbol{P}_f(\boldsymbol{\gamma}) \equiv [P_f^{(0)}(\gamma_0), P_f^{(1)}(\gamma_1), \ldots, P_f^{(K-1)}(\gamma_{K-1})]^T \tag{2.29}$$

$$\boldsymbol{P}_m(\boldsymbol{\gamma}) \equiv [P_m^{(0)}(\gamma_0), P_m^{(1)}(\gamma_1), \ldots, P_m^{(K-1)}(\gamma_{K-1})]^T \tag{2.30}$$

In the present context of CRs, the probability of missed detection, i.e., $P_m^{(k)}(\gamma_k) = 1 - P_d^{(k)}(\gamma_k)$, represents the likelihood of the SU's interfering with any EU in the k-th subband. Furthermore, $1 - P_f^{(k)}$ is a measure of the likelihood of detecting and, hence, using a spectrum hole. If r_k is used to denote the achievable throughput in the k-th subband and $\boldsymbol{r} \equiv [r_0, r_1, \ldots, r_{K-1}]^T$ denotes

[3]Some discrepancies were found in the computation of $\mathit{Var}[Y_k]$ in [12]. These have been corrected here. Further details can be found in Appendix B.

the set of throughputs for the K subbands, the *aggregate opportunistic throughput* of the SU can be defined as [12]:

$$R(\boldsymbol{\gamma}) \triangleq \boldsymbol{r}^T[\mathbf{1} - \boldsymbol{P}_f(\boldsymbol{\gamma})] \tag{2.31}$$

In principle, the quantity r_k can be calculated using Shannon's capacity formula as the maximum theoretic data rate achievable in the k-th subband (see [29]).

Conversely, consider a case where one or more EUs are using the system. Let c_k denote the cost of interfering with the EU(s) in the k-th subband and vector $\boldsymbol{c} \triangleq [c_0, c_1, \ldots, c_{K-1}]^T$ represent the costs associated with interfering in the K subbands. Since the probability of missed detection is a measure of the likelihood of interfering with the EU(s), the *aggregate interference* added by the SU (to all the EUs) can be defined as [12]:

$$C(\boldsymbol{\gamma}) \triangleq \boldsymbol{c}^T \boldsymbol{P}_m(\boldsymbol{\gamma}) \tag{2.32}$$

If the detection is carried out in the Neyman-Pearson framework, the goal is to find the optimum threshold $\hat{\gamma}_k$ for the k-th subband that minimizes $P_m^{(k)}$ given an upper bound on $P_f^{(k)} \leq \beta_k$. However, given different interference costs, c_k, and Shannon capacities, r_k for different subbands, band-by-band optimization of thresholds proves to be a sub-optimal solution. Instead, the objective of [12] is to find an optimal set of thresholds $\{\gamma_k\}_{k=0}^{K-1}$ that achieves one of the following:

- Maximization of the aggregate opportunistic throughput with constraint on the aggregate

interference[4]:

$$\max_{\boldsymbol{\gamma}} \quad R(\boldsymbol{\gamma}) \tag{2.33a}$$

$$\text{s.t.} \quad \boldsymbol{c}^T \boldsymbol{P}_m(\boldsymbol{\gamma}) \leq \epsilon \tag{2.33b}$$

$$\boldsymbol{P}_m(\boldsymbol{\gamma}) \leq \boldsymbol{\alpha} \tag{2.33c}$$

$$\boldsymbol{P}_f(\boldsymbol{\gamma}) \leq \boldsymbol{\beta} \tag{2.33d}$$

- Minimization of the aggregate interference with constraint on the aggregate opportunistic throughput:

$$\min_{\boldsymbol{\gamma}} \quad C(\boldsymbol{\gamma}) \tag{2.34a}$$

$$\text{s.t.} \quad \boldsymbol{r}^T[\mathbf{1} - \boldsymbol{P}_f(\boldsymbol{\gamma})] \geq \delta \tag{2.34b}$$

$$\boldsymbol{P}_m(\boldsymbol{\gamma}) \leq \boldsymbol{\alpha} \tag{2.34c}$$

$$\boldsymbol{P}_f(\boldsymbol{\gamma}) \leq \boldsymbol{\beta} \tag{2.34d}$$

where $\boldsymbol{\alpha} = [\alpha_0, \alpha_1, \ldots, \alpha_{K-1}]^T$ are the interference limits for the K subbands and $\boldsymbol{\beta} = [\beta_0, \beta_1, \ldots, \beta_{K-1}]^T$; the mimimum opportunistic spectrum utilization is represented by $\mathbf{1} - \boldsymbol{\beta} = [1-\beta_0, 1-\beta_1, \ldots, 1-\beta_{K-1}]^T$. Both the objective and constraint functions above are generally non-convex. However, by carefully analyzing the problem, the search of the optimum solution can be simplified. Firstly, the fact that the Q-function is monotonically non-increasing, in conjunction (2.26) and (2.27), allows the constraints in (2.33c) - (2.34d) to be transformed into a

[4]It is possible to extend this formulation to the case where a number J of EUs are using the system, with the j-th EU occupying a subset S_j of the K subbands, and to contain the total interference to any specific EU, i.e., $\sum_{i \in S_j} c_i P_m^{(i)}(\gamma_i) < \epsilon_j$ for $j = 0, 1, \ldots, J-1$. However, we do not consider this scenario in this work; see [12].

linear constraint:

$$\gamma_{min,k} \leq \gamma_k \leq \gamma_{max,k}$$

where:

$$\gamma_{min,k} \triangleq \sigma_v^2 \Big[M + \sqrt{M} Q^{-1}(\beta_k) \Big]$$
$$\gamma_{max,k} \triangleq (\sigma_v^2 + |H_k|^2) \Big[M + \sqrt{M} Q^{-1}(1 - \alpha_k) \Big]$$

Secondly, it can be shown that the functions $P_f^{(k)}(\gamma_k)$ and $P_m^{(k)}(\gamma_k)$ are both convex in γ_k if $P_f^{(k)}(\gamma_k) \leq 0.5$ and $P_m^{(k)}(\gamma_k) \leq 0.5$. Accordingly, the above optimization problems are convex when properly restricted to the corresponding feasible set. To this end, the parameters α_k and β_k must lie in $[0, \frac{1}{2}]$.

Therefore, the multiband joint optimization problems may be simplified to:

- Maximization of the aggregate opportunistic throughput with constraint on the aggregate interference:

$$\begin{aligned} \max_{\boldsymbol{\gamma}} \quad & R(\boldsymbol{\gamma}) \\ \text{s.t.} \quad & \boldsymbol{c}^T \boldsymbol{P}_m(\boldsymbol{\gamma}) \leq \epsilon \\ & \gamma_{min,k} \leq \gamma_k \leq \gamma_{max,k} \end{aligned} \tag{2.35}$$

- Minimization of the aggregate interference with constraint on the aggregate opportunistic

throughput:

$$\begin{aligned} \min_{\boldsymbol{\gamma}} \quad & C(\boldsymbol{\gamma}) \\ \text{s.t.} \quad & \boldsymbol{r}^T[\mathbf{1} - \boldsymbol{P}_f(\boldsymbol{\gamma})] \geq \delta \\ & \gamma_{min,k} \leq \gamma_k \leq \gamma_{max,k} \end{aligned} \tag{2.36}$$

Reproduced results of the above optimizations will be presented in Section 5.2 for reference in our study.

2.2.2 Collaborative Multiband Joint Detection

Although single-user detection, as described in Section 2.2.1, can satisfy the requirements of spectrum sensing applications, it performs poorly in the presence of blockage effects, such as multipath fading. In such conditions, use of collaborative detection, whereby a network of co-operating SUs (i.e., CR detectors) share information, demonstrates better robustness. In this section, such a scheme is discussed. The procedure described in this section is analogous to what was presented in section 2.2.1 and uses similar notations.

Consider a case where a number N of SUs collaborate to perform spectrum sensing. Using notations similar to those used in Section 2.2.1, the signal observed by the n-th SU in the k-th subband during the m-th time frame can be represented as:

$$\begin{aligned} \mathcal{H}_{0,k} &: R_k^n(m) = V_k^n(m) \\ \mathcal{H}_{1,k} &: R_k^n(m) = H_k^n S_k(m) + V_k^n(m) \end{aligned}$$

$Y_k^n \triangleq \sum_{m=0}^{M-1} |R_k^n(m)|^2$ is the n-th SU's observed energy in the k-th subband. For the k-th subband, we define a vector $\mathbf{Y}_k = [Y_k^0, Y_k^1, \ldots, Y_k^{N-1}]^T$, which consists of energy measurements

from all N SUs. Consequently, the following test statistic can be computed using a linear fusion scheme to combine the energy measurements of the N collaborating SUs:

$$Z_k = \sum_{n=0}^{N-1} w_k^n Y_k^n = \boldsymbol{w}_k^T \boldsymbol{Y}_k \tag{2.37}$$

where $\boldsymbol{w}_k = [w_k^0, w_k^1, \ldots, w_k^{N-1}]^T$ are the corresponding weight coefficients used for the subband k. The weight vectors for different subbands may be concatenated to construct a weight matrix: $W = [\boldsymbol{w}_0 | \boldsymbol{w}_1 | \ldots | \boldsymbol{w}_{K-1}]$. Note that the individual weights $w_k^n \geq 0$.

The following decision rule is now used for the k-th subband:

$$Z_k \underset{\mathcal{H}_{0,k}}{\overset{\mathcal{H}_{1,k}}{\gtrless}} \gamma_k, \quad k = 0, 1, \ldots, K-1 \tag{2.38}$$

As before, the central limit theorem dictates that for a large enough number of samples M, Z_k is approximately normally distributed with mean:

$$E[Z_k] = \begin{cases} M \boldsymbol{w}_k^T \sigma_v^2 \mathbf{1}, & \mathcal{H}_{0,k} \\ M \boldsymbol{w}_k^T (\sigma_v^2 \mathbf{1} + \boldsymbol{G}_k), & \mathcal{H}_{1,k} \end{cases} \tag{2.39}$$

and variance:

$$\mathit{Var}[Z_k] = \begin{cases} M \boldsymbol{w}_k^T \sigma_v^4 \boldsymbol{w}_k, & \mathcal{H}_{0,k} \\ M \boldsymbol{w}_k^T \Sigma_k \boldsymbol{w}_k & \mathcal{H}_{1,k} \end{cases} \tag{2.40}$$

where $\mathbf{1} = [1, 1, \ldots, 1]^T$, $\boldsymbol{G}_k = [|H_k^0|^2, |H_k^1|^2, \ldots, |H_k^{N-1}|^2]$ is the vector of channel squared magnitude responses between the EU and the N collaborating SUs, and $\Sigma_k = \sigma_v^4 I_N + 2\sigma_v^2 \mathrm{diag}\{\boldsymbol{G}_k\} + [\mathrm{diag}\{\boldsymbol{G}_k\}]^2$.

On this basis, the probabilities of false alarm and detection associated with (2.38) can be

computed as:

$$P_f^{(k)}(\gamma_k) = Pr(Y_k > \gamma_k | \mathcal{H}_{0,k}) = Q\left(\frac{\gamma_k - M\boldsymbol{w}_k^T\sigma_v^2\mathbf{1}}{\sqrt{M\boldsymbol{w}_k^T\sigma_v^4\boldsymbol{w}_k}}\right) \tag{2.41}$$

$$P_d^{(k)}(\gamma_k) = Pr(Y_k > \gamma_k | \mathcal{H}_{1,k}) = Q\left(\frac{\gamma_k - M\boldsymbol{w}_k^T(\sigma_v^2\mathbf{1} + \boldsymbol{G}_k)}{\sqrt{M\boldsymbol{w}_k^T\Sigma_k\boldsymbol{w}_k}}\right) \tag{2.42}$$

As was done in the case of single-user detection case, by defining a cost vector, $\boldsymbol{c} = [c_0, c_1, \ldots, c_{K-1}]^T$, comprising of the costs of adding interference in each of the K subbands, and a Shannon capacity vector, $\boldsymbol{r} = [r_0, r_1, \ldots, r_{K-1}]^T$, we can define the performance metrics for the collaborative joint detection framework. In particularly, the aggregate opportunistic throughput is defined as:

$$R(W, \boldsymbol{\gamma}) \triangleq \boldsymbol{r}^T[\mathbf{1} - \boldsymbol{P}_f(W, \boldsymbol{\gamma})] \tag{2.43}$$

and the aggregate interference is defined as:

$$C(W, \boldsymbol{\gamma}) \triangleq \boldsymbol{c}^T\boldsymbol{P}_m(W, \boldsymbol{\gamma}) \tag{2.44}$$

where the dependence on the weight matrix has been made explicit. It is now possible to formulate global optimization problems in order to find a set of thresholds $\{\gamma_k\}_{k=0}^{K-1}$ and a set of fusion weights $\{\boldsymbol{w}_k\}_{k=0}^{K-1}$ that achieve one of the following:

- Maximization of the aggregate opportunistic throughput with constraint on the aggregate interference;
- Minimization of the aggregate interference with constraint on the aggregate opportunistic

throughput.

The resulting problems are similar to those in (2.33) and (2.34), except for the explicit dependence of $\boldsymbol{P}_f$, $\boldsymbol{P}_f$, R and C on W.

As in the previous section, the resulting objective and constraint functions above are non-convex in general. Therefore, it is necessary to limit the search to suitable feasible sets. Moreover, in the spatially distributed case, in addition to the optimum set of thresholds, $\{\gamma_k\}_{k=0}^{K-1}$, the optimum set of weight vectors, $\{\boldsymbol{w}_k\}_{k=0}^{K-1}$, has to be computed as well. [12] shows that the optimum weight vector is given by:

$$\boldsymbol{w}_k^o = \frac{\Sigma_k^{-1}\boldsymbol{G}_k}{\|\Sigma_k^{-1}\boldsymbol{G}_k\|_2} \tag{2.45}$$

In order to simplify the spectral optimization problem, once again, the fact that the Q-function is monotonically non-increasing is exploited to transform (2.33c) - (2.33d) into a linear constraint:

$$\gamma_{min,k} \leq \gamma_k \leq \gamma_{max,k}$$

where, this time:

$$\gamma_{min,k} \triangleq M\sigma_v^2\mathbf{1}^T\boldsymbol{w}_k^o + Q^{-1}(\beta_k)\sqrt{M\boldsymbol{w}_k^{oT}\sigma_v^4\boldsymbol{w}_k^o}$$
$$\gamma_{max,k} \triangleq M(\sigma_v^2\mathbf{1} + \boldsymbol{G}_k)^T\boldsymbol{w}_k^o + Q^{-1}(1-\alpha_k)\sqrt{M\boldsymbol{w}_k^{oT}\Sigma_k\boldsymbol{w}_k^o}$$

As in Section 2.2.1, the simplified optimization problems will be convex if parameters α_k and β_k are restricted to $[0, \frac{1}{2}]$.

Therefore, the spatial-spectral optimization problems may be formulated as:

- Maximization of the aggregate opportunistic throughput with constraint on the aggregate

interference:

$$\begin{aligned} \max_{\boldsymbol{\gamma}} \quad & R(W^o, \boldsymbol{\gamma}) \\ \text{s.t.} \quad & \boldsymbol{c}^T \boldsymbol{P}_m(\boldsymbol{\gamma}) \leq \epsilon \\ & \gamma_{min,k} \leq \gamma_k \leq \gamma_{max,k} \end{aligned} \tag{2.46}$$

- Minimization of the aggregate interference with constraint on the aggregate opportunistic throughput:

$$\begin{aligned} \min_{\boldsymbol{\gamma}} \quad & C(W^o, \boldsymbol{\gamma}) \\ \text{s.t.} \quad & \boldsymbol{r}^T [\mathbf{1} - \boldsymbol{P}_f(W^o, \boldsymbol{\gamma})] \geq \delta \\ & \gamma_{min,k} \leq \gamma_k \leq \gamma_{max,k} \end{aligned} \tag{2.47}$$

2.3 Final Remark

The detection schemes presented in this section assume that the occupany of any particular subband is independent of that of the other subbands. In general, as discussed in Section 3.1, this assumption does not hold true. As will be shown in Chapter 4, it is possible to exploit *a priori* knowledge of the correlation between subband occupany to improve spectrum sensing performance in multiband joint detection frameworks. In the next two chapters, detection schemes that exploit such *a priori* knowledge of correlation are discussed, starting with the development of improved detectors of multiband channel occupancy in Chapter 3 and their application to extend the work of [12] in Chapter 4.

Chapter 3

Optimum Detectors of Multiband Channel Occupancy

In this chapter, the optimum detectors of the multiband channel occupancy are developed. We present an occupancy model to characterize the wideband signal observed by the SU using an underlying occupancy vector. First, considering a Bayesian framework, the MAP estimator of the occupancy vector is developed. However, the MAP estimator proves to be computationally intractable. Consequently, a lower-complexity detector of the occupancy vector that relies only on optimal linear combination of subband energy measurements is constructed and analyzed.

3.1 Model for Multiband Channel Occupany

As in Section 2.2.1, the wideband signal observed by the SU (i.e., CR detector) after down-conversion and uniform sampling, denoted by$r(n)$, is expressed as:

$$r(n) = \sum_{l=0}^{L-1} h(l)s(n-l) + v(n) \tag{3.1}$$

where $s(n)$ is the EU signal, $h(n)$ is the impulse response of the wireless channel between the EU and SU (assumed to be time-invariant), L is the length of $h(n)$ and $v(n)$ is an additive noise term. Using a K-point discrete Fourier Transform (DFT), successive frames of $r(n)$ are decomposed into narrow-band discrete frequency components, i.e.:

$$R_k(m) = \sum_{n=0}^{K-1} r(mK+n)e^{-j2\pi nk/K},\ k = 0, 1, \ldots, K-1 \tag{3.2}$$

where k is the frequency index, $m = 0, 1, \ldots, M-1$ is the frame index and M is the number of frames available. As before, H_k, $S_k(m)$ and $V_k(m)$ denote the k-th DFT coefficients of $h(n)$, $s(mK+n)$ and $v(mK+n)$, respectively. Assuming a large time-bandwidth product ($K > L$), the convolution in (3.1) maps into a product of the DFT coefficients of the corresponding quantities. Accordingly, we can represent the m-th sample of the observed signal in the k-th subband as:

$$R_k(m) = H_k S_k(m) + V_k(m), \quad k = 0, 1, \ldots, K-1. \tag{3.3}$$

The sequence of EU signal samples, $\{S_k(m)\}$, and of background noise samples, $\{V_k(m)\}$, are modelled as independent random processes. Given a particular state of occupancy of the wideband channel, samples from each process are assumed to be independent across frequency and frame indices and to obey a zero-mean complex circular symmetric Gaussian distribution. The noise variance, $\sigma_v^2 \triangleq E[|V_k(m)|^2]$, and the channel squared magnitude response, $G_k \triangleq |H_k|^2$, are assumed to be known from *a priori* estimation. Without loss in generality, we set $E[|S_k(m)|^2] = 1$, if the k-th subband is occupied and 0 otherwise. Note that this corresponds to the occupancy model being used in current literature, such as the one described in (2.22). Indeed, in the absence of an EU, $E[|S_k(m)|^2] = 0$ and (3.3) reduces to $R_k(m) = V_k(m)$.

In this thesis, we adopt a Bayesian framework and model the occupancy of the k-th subband as a binary random variable, B_k, with realization $b_k \in \{0, 1\}$. As above, 0 and 1 respectively

indicate an empty and occupied subband; accordingly, we have $E[|S_k(m)|^2 \big| B_k = b_k] = b_k$. The wideband spectrum occupancy may then be described by the random vector

$$\mathbf{B} = [B_0, B_1, \ldots, B_{K-1}]^T \tag{3.4}$$

with realizations $\mathbf{b} = [b_0, b_1, \ldots, b_{K-1}]^T \in \{0,1\}^K$. The joint probability mass function (PMF) of $\mathbf{B}$ is denoted by $P_{\mathbf{B}}(\mathbf{b}) = \Pr(B_0 = b_0, \ldots, B_{K-1} = b_{K-1})$. Additionally, we define the mean vector $\boldsymbol{\mu} = E[\mathbf{B}]$, with entries $\mu_i = E[B_i]$, and the correlation matrix $\boldsymbol{\Lambda} = E[\mathbf{B}\mathbf{B}^T]$, with entries $\lambda_{ij} = E[B_i B_j]$. The occupancy vector $\mathbf{B}$ is assumed to be independent of $\{V_k(m)\}$ and to remain unchanged during the detection interval.

Given the above signal model and observed time-frequency data in (3.3), we seek an efficient detector structure that will enable the SU to determine the state of occupancy of the wideband channel respresented by the random vector $\boldsymbol{B}$. Under the conventional assumption of independent subband occupancy, the solution to this problem amounts to comparing the received signal energy in each subband to a decision threshold, i.e., K decoupled binary tests. Here, we consider the general situation in which the occupancy variables B_i and B_j may not be independent for $i \neq j$. For instance, because of spectral allocation plan, an EU (such as WLAN or broadcast television) may be transmitting over a wideband spectrum, which maps to multiple subbands for the SU; or, as discussed in [16], a contiguous section of the wireless spectrum licensed to the EU may be deeply faded due to multipath fading effects. In this situation, EU detection in the faded subbands is difficult, but there exists a correlation between the occupancies of the faded and unfaded subbands. We will show in this thesis that significant gains may be achieved in detection performance if such *a priori* knowledge of correlation is exploited.

3.2 Bayesian Estimation of Channel Occupancy Vector

Given the model described in Section 3.1, the mean and variance of $R_k(m)$ conditioned on $B_k = b_k$ are given by:

$$E[R_k(m)\big|B_k = b_k] = 0 \tag{3.5}$$

$$Var[R_k(m)\big|B_k = b_k] = b_k G_k + \sigma_v^2 \tag{3.6}$$

Let $\boldsymbol{R}$ denote a random vector containing the complete set of observed data in (3.3), i.e.: $\boldsymbol{R} = [\boldsymbol{R}_0^T, \boldsymbol{R}_1^T, \ldots, \boldsymbol{R}_{K-1}^T]^T$, where $\boldsymbol{R}_k = [R_k(0), R_k(1), \ldots, R_k(M-1)]^T$, with corresponding realization $\boldsymbol{r} = [\boldsymbol{r}_0^T, \boldsymbol{r}_1^T, \ldots, \boldsymbol{r}_{K-1}^T]^T$, where $\boldsymbol{r}_k = [r_k(0), r_k(1), \ldots, r_k(M-1)]^T$. Consequently, the conditional probability density function (PDF) of $\boldsymbol{r}$ given $\boldsymbol{B} = \boldsymbol{b}$ can be written as:

$$f_{\boldsymbol{R}|\boldsymbol{B}}(\boldsymbol{r}|\boldsymbol{b}) = \prod_{m=0}^{M-1} \prod_{k=0}^{K-1} \frac{1}{\pi(b_k G_k + \sigma_v^2)} \exp\Big\{-\frac{|r_k(m)|^2}{b_k G_k + \sigma_v^2}\Big\} \tag{3.7}$$

Using (3.7), the MAP estimator of $\boldsymbol{B}$ given the observation $\boldsymbol{R} = \boldsymbol{r}$ can be formulated as:

$$\hat{\boldsymbol{B}}_{\text{MAP}} = \arg\max_{\boldsymbol{b}} L_{\text{MAP}}(\boldsymbol{b}|\boldsymbol{r}) \tag{3.8}$$

The associated log-likelihood function is given by:

$$L_{\text{MAP}}(\boldsymbol{b}|\boldsymbol{r}) = \ln P_{\boldsymbol{B}}(\boldsymbol{b}) - M \sum_{k=0}^{K-1} \ln(b_k G_k + \sigma_v^2) - \sum_{k=0}^{K-1} \frac{y_k}{b_k G_k + \sigma_v^2} \tag{3.9}$$

where y_k is the energy measured in the k-th subband over M frames and is defined as:

$$y_k = \sum_{m=0}^{M-1} |r_k(m)|^2 \tag{3.10}$$

In the next subsections, we consider, by way of example, special cases of occupancy vector $\boldsymbol{B}$ models to illustrate the use and complexity of the optimum Bayesian estimator of spectrum occupancy in (3.8).

3.2.1 Estimation of Channel Occupancy for $K = 2$ Case

In order to illustrate the use of (3.8) to estimate the channel state of occupancy, we first consider a lower dimensionality situation with $K = 2$ subbands. In this case, the wideband channel occupancy is represented by $\boldsymbol{B} = [B_0, B_1]^T$ with possible realizations $[0, 0]^T$, $[0, 1]^T$, $[1, 0]^T$ and $[1, 1]^T$. The observed data can be denoted using $\boldsymbol{R} = [\boldsymbol{R}_0^T, \boldsymbol{R}_1^T]^T$ and the energies measured in the 0^{th} and 1^{st} subbands are denoted using y_0 and y_1 respectively. By evaluating the log-likelihood function (3.9) for each of the four possible realizations, it is possible to construct a decision diagram in the (y_0, y_1) plane, such as the one shown in Figure 3.1.

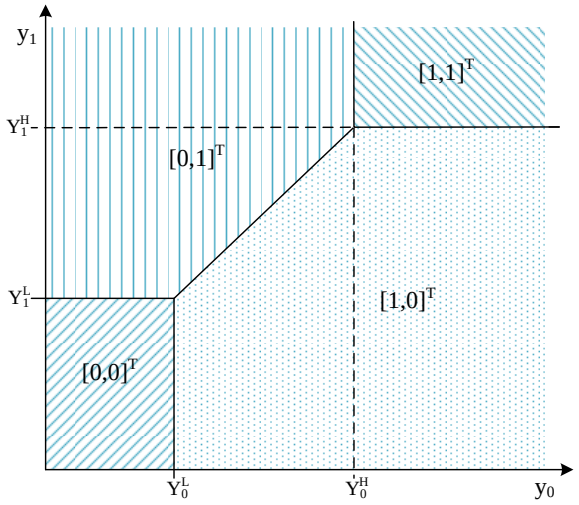

Figure 3.1 Decision regions of the MAP estimator for $K = 2$

The labels associated with the decision boundaries are defined as follows:

$$Y_0^L = \sigma_v^2\Big(1+\frac{\sigma_v^2}{G_0}\Big)\left[M\ln\Big(1+\frac{G_0}{\sigma_v^2}\Big)+\ln\frac{P_{\boldsymbol{B}}(0,0)}{P_{\boldsymbol{B}}(1,0)}\right] \tag{3.11}$$

$$Y_0^H = \sigma_v^2\Big(1+\frac{\sigma_v^2}{G_0}\Big)\left[M\ln\Big(1+\frac{G_0}{\sigma_v^2}\Big)+\ln\frac{P_{\boldsymbol{B}}(0,1)}{P_{\boldsymbol{B}}(1,1)}\right] \tag{3.12}$$

$$Y_1^L = \sigma_v^2\Big(1+\frac{\sigma_v^2}{G_1}\Big)\left[M\ln\Big(1+\frac{G_1}{\sigma_v^2}\Big)+\ln\frac{P_{\boldsymbol{B}}(0,0)}{P_{\boldsymbol{B}}(0,1)}\right] \tag{3.13}$$

$$Y_1^H = \sigma_v^2\Big(1+\frac{\sigma_v^2}{G_1}\Big)\left[M\ln\Big(1+\frac{G_1}{\sigma_v^2}\Big)+\ln\frac{P_{\boldsymbol{B}}(1,0)}{P_{\boldsymbol{B}}(1,1)}\right] \tag{3.14}$$

For instance, if the pair of measured energies (y_0, y_1) falls in the region labelled $[1,0]^T$, then the MAP detector will decide in favour of subband 0 being occupied ($y_0 > Y_0^L$) and subband 1 being unoccupied ($y_1 < Y_1^H$).

In general, for K subbands, the size of the sample space, i.e., the number of distinct integer vector elements $\boldsymbol{b}$, is 2^K. Therefore, although the MAP estimator leads to simple decision regions such as those in Figure 3.1 for low dimensionality, for higher number of subbands, such constructions have to be done in K dimensional space, making the process computationally complex.

3.2.2 Estimation of Channel Occupancy for Uncorrelated Case

Here we consider the special case where the subband occupancies are independent of each other, i.e., $P_{\boldsymbol{B}}(\boldsymbol{b}) = \prod_{k=0}^{K-1} P_{B_k}(b_k)$, where $P_{B_k}(b_k) = \Pr(B_k = b_k)$ denotes the marginal probability of occupancy of the k-th subband. The maximization in (3.9) can then be done independently for each k, i.e., $\hat{B}_k = \arg\max_{b_k} L_k(b_k|r_k)$ where:

$$L_k(b_k|r_k) = \ln P_{B_k}(b_k) - M\ln(b_k G_k + \sigma_v^2) - \frac{y_k}{b_k G_k + \sigma_v^2} \tag{3.15}$$

Maximization of (3.15) leads to an independent binary hypothesis test for each subband:

$$y_k \underset{\mathcal{H}_{0,k}}{\overset{\mathcal{H}_{1,k}}{\gtrless}} \gamma_k, \quad k = 0, 1, \ldots, K-1 \tag{3.16}$$

where γ_k is the threshold parameter used in the k-th subband. Present literature largely deals with this special case where the optimal multiband detector consists of K parallel decoupled narrowband ones.

However, as pointed out earlier, the occupancy of ajacent subbands is likely to be correlated in practice, i.e., the random variable B_k will not be statistically independent. In the general case where the subband occupancies B_k are not independent of each other, (3.9) leads to a non-linear integer optimization in K-dimensional space. As we can infer from the example in Subsection 3.2.1, this is a computationally challenging problem with intricate decision regions whose complexity grows exponentially with the number of subbands K. Therefore, to solve the multiband energy detection problem with correlated subband occupancy within reasonable limits of processing time and complexity, we need a simpler detector structure, such as the one discussed next.

3.3 Optimum Linear Energy Combiner (OLEC) Detector

From (3.9), we note that the measured energies $\{y_k\}_{k=0}^{K-1}$ define a set of sufficient statistics for the MAP estimator. Furthermore, only linear processing of these quantities is required. However, since the weights applied to the energies $\{y_k\}_{k=0}^{K-1}$ depend on the particular hypothesis being tested, 2^K linear combiners are needed in order to obtain the MAP estimator. This exponential growth in complexity of the MAP estimator motivates the use of simpler detector structures. In particular, we investigate here a simplified detector structure in which subband energies are

linearly combined, using one combiner per subband, and a hypothesis test is carried out on the resulting statistic for each subband.

Specifically, we let

$$\hat{B}_k = \boldsymbol{\xi}_k^T \boldsymbol{Y} + \epsilon_k \tag{3.17}$$

denote an estimate of the unknown occupancy B_k of the k-th subband, as obtained by an affine transformation on the random energy vector $\boldsymbol{Y} = [Y_0, Y_1, \ldots, Y_{K-1}]^T$, where

$$Y_k = \sum_{m=0}^{M-1} |R_k(m)|^2 \tag{3.18}$$

We propose to compute the optimum weight vector $\boldsymbol{\xi}_k$ and constant ϵ_k in (3.17) as the minimizer of the MSE defined as:

$$J(\boldsymbol{\xi}_k, \epsilon_k) = E[(\hat{B}_k - B_k)^2] \tag{3.19}$$

$$= E[(\boldsymbol{\xi}_k^T \boldsymbol{Y} + \epsilon_k - B_k)^2] \tag{3.20}$$

As shown in Appendix A, the MMSE weight vector is found to be:

$$\boldsymbol{\xi}_k^o = E[\tilde{\boldsymbol{Y}} \tilde{\boldsymbol{Y}}^T]^{-1} E[\tilde{\boldsymbol{Y}} \tilde{B}_k] \tag{3.21}$$

where we define the centred quantities $\tilde{\boldsymbol{Y}} = \boldsymbol{Y} - E[\boldsymbol{Y}]$ and $\tilde{B}_k = B_k - \mu_k$. The optimum value of ϵ_k, given by $\epsilon_k^o = \mu_k - \boldsymbol{\xi}_k^{oT} E[\boldsymbol{Y}]$, is needed in the MMSE estimation of B_k since the latter has non-zero mean.

Substituting (3.3) into (3.18) and making use of the modelling assumptions in Section 3.1, we can show that[1]:

[1] Further details can be found in Appendix B.

$$E[\tilde{Y}_i \tilde{B}_k] = M(\lambda_{ik} - \mu_i \mu_k) G_i \tag{3.22}$$

$$E[\tilde{Y}_i \tilde{Y}_j] = M^2(\lambda_{ij} - \mu_i \mu_j) G_i G_j + M(\mu_i G_i^2 + 2\mu_i G_i \sigma_v^2 + \sigma_v^4)\delta_{ij} \tag{3.23}$$

These moments, which are needed to evaluate the MMSE weight vector in (3.21), depend on the following parameters:

- M, the number of frames being processed;
- μ_i and λ_{ij}, the 1st and 2nd moments of the occupancy vector $\boldsymbol{B}$;
- G_i, the channel gain; and
- σ_v^2, the background noise power.

We assume that these quantities are known a priori. The resulting multiband detector structure,

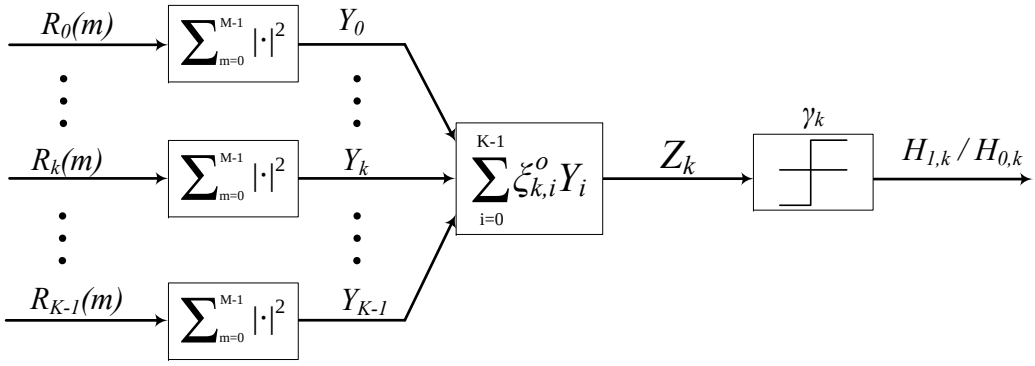

Figure 3.2 Single block of the optimum linear energy combiner (only the detector for the k-th subband is shown)

illustrated in Figure 3.2 for the k-th subband, amounts to implementing the following test:

$$Z_k = \boldsymbol{\xi}_k^{oT} \boldsymbol{Y} \underset{\mathcal{H}_{0,k}}{\overset{\mathcal{H}_{1,k}}{\gtrless}} \gamma_k, \quad k = 0, 1, \ldots, K-1 \tag{3.24}$$

where Z_k represents the output of the optimum linear energy combiner. That is, if $Z_k > \gamma_k$, we decide in favour of $\mathcal{H}_{1,k}$, i.e., the k-th subband is occupied, while, if $Z_k < \gamma_k$, we decide in favour

of $\mathcal{H}_{0,k}$, i.e., the k-th subband is unoccupied. The bias term ϵ_k^o is not shown in Figure 3.2 as it is absorbed in the detection threshold γ_k. Also, $\boldsymbol{\xi}_k^o$ can be normalized such that $\xi_{kk}^o = 1$.

Note that the weights $\boldsymbol{\xi}_k^o$ were chosen to minimize the MSE in detection for the class of detectors based on linear energy combination, thereby making the detector in (3.24) optimal in the MMSE sense. Some cases of sub-optimal linear energy combiners are presented in Section 3.3.1 below.

To exploit spatial diversity, linear combination of energies measured within a given subband by spatially distributed CRs has been applied to distributed sensing, e.g., in [13]. The proposed approach here is different in that it attempts to optimally combine the energies measured by a single CR across multiple subbands based on the correlation between the subband occupancies of EUs. In fact, as will be shown in Sections 4.2 and 5.2.2, the OLEC detector in (3.24) can be used to improve the performance of collaborative detection schemes, such as those in [12] and [13].

3.3.1 Lower Dimensionality Energy Combiners

For certain subband occupancy models used in current literature, for example, [16], where the degree of correlation between B_j and B_k decreases as the frequency separation $|k-i|$ increases, we find that the relative weights ξ_{ki}^o given to Y_i in the computation of Z_k decreases in a similar way. Consequently, the greatest amount of weight is placed on the energy measurements of the current and adjacent subbands, with indices k and $k \pm 1$. This suggests the consideration of a simplified, sub-optimal linear combiner structure in which the sufficient statistic used by the binary detector in the k-th subband is obtained from[2]:

$$Z_k^{\pm} = Y_k + \eta_- Y_{k-1} + \eta_+ Y_{k+1} \tag{3.25}$$

[2]With obvious modifications for the edge frequencies $k = 0$ and $K-1$.

where the gains $\eta_{\pm}$ can be chosen in a number of different ways, such as:

- Truncation of the optimum solution (3.21);
- Solution of a simplified (3-dimensional) version of the MMSE problem; or
- Minimization of the probability of missed detection for a given probability of false alarm.

Some of these options will be considered in connection with our simulation experiments reported in Section 5.1.

3.3.2 Performance of the OLEC Detector

For detection tasks based on hypothesis-testing, the minimum attainable probability of missed detection for a given upper limit on the probability of false alarm is generally used as an objective measure of the performance. Here, we compute these probabilities for the OLEC detector developed above. First, conditioned on $B_k = b_k$, the mean and variance of the test statistic (3.24) can be expressed as:

$$E[Z_k|B_k = b_k] = \boldsymbol{\xi}_k^{oT} E[\boldsymbol{Y}|B_k = b_k] \tag{3.26}$$

$$Var[Z_k|B_k = b_k] = \boldsymbol{\xi}_k^{oT} E[\tilde{\boldsymbol{Y}}\tilde{\boldsymbol{Y}}^T|B_k = b_k]\boldsymbol{\xi}_k^{o} \tag{3.27}$$

By extending the derivations for the unconditional mean and correlation of $\boldsymbol{Y}$ presented in Appendix B, it can be shown that:

$$E[Y_i|B_k = b_k] = M(\mu_{i|k}G_i + \sigma_v^2) \tag{3.28}$$

$$E[\tilde{Y}_i\tilde{Y}_j|B_k = b_k] = M^2 G_i G_j(\lambda_{ij|k} - \mu_{i|k}\mu_{j|k}) + M[\mu_{i|k}G_i(G_i + 2\sigma_v^2) + \sigma_v^4]\delta_{ij} \tag{3.29}$$

where the following short-hand notations are used for convenience:

$$\mu_{i|k} \equiv E[B_i|B_k = b_k] \tag{3.30}$$

$$\lambda_{ij|k} \equiv E[B_i B_j|B_k = b_k] \tag{3.31}$$

According to the central limit theorem [30], for a sufficiently large number of frames M, it is reasonable to assume that the random variables Y_k in (3.18) are normally distributed under each of the hypotheses. In turn, this implies that the linearly combined output Z_k in (3.24) is also normally distributed under each of the hypotheses. Consequently, the probability of false alarm and the probability of missed detection associated with the test in (3.24) are given by:

$$P_f^{(k)}(\gamma_k, \boldsymbol{\xi}_k^o) = Q\left(\frac{\gamma_k - E[Z_k|B_k = 0]}{\sqrt{Var[Z_k|B_k = 0]}}\right) \tag{3.32}$$

$$P_m^{(k)}(\gamma_k, \boldsymbol{\xi}_k^o) = 1 - Q\left(\frac{\gamma_k - E[Z_k|B_k = 1]}{\sqrt{Var[Z_k|B_k = 1]}}\right) \tag{3.33}$$

where the conditional mean and variance are as calculated in (3.26)-(3.31). Note that the above expressions hold true for hypothesis tests carried out on $Z_k^{\pm}$ defined in (3.25) if $\boldsymbol{\xi}_k^o$ is replaced by $\boldsymbol{\xi}_k^{\pm} = [0, \ldots, 0, \eta_-, 1, \eta_+, 0, \ldots, 0]^T$. To evaluate the probabilities in (3.32) and (3.33), knowledge of the conditional moments, $\mu_{i|k}$ and $\lambda_{ij|k}$, is needed. These quantities can be obtained from measurements of subband occupancies by EUs, or from a suitable occupancy model, as shown in Chapter 5.

Chapter 4

Multiband Joint Detection with the Optimum Linear Energy Combiner

As discussed in Section 1.1, multiband joint energy detection has gained importance in the context of spectrum sensing for cognitive radios. In Section 2.2, we presented detailed examples of contemporary spectrum sensing techniques in both single-user and collaborative multiband joint detection frameworks. We noted that even in such sophisticated sensing schemes, current literature assumes the subband occupancies to be independent of each other. In this section, we show how we can exploit *a priori* knowledge of correlation between subband occupancies in order to obtain significant performance gains in multiband joint detection tasks. Here, we consider the use of the OLEC detector, developed in Section 3.3, within the multiband joint detection scheme presented in [12]. First, the OLEC is applied to single-user multiband joint detection. Then, the OLEC is adapted for the multi-user collaborative detection case as well.

4.1 Single-User Multiband Joint Detection

We begin with the occupancy model developed in Section 3.1. Following a K-point discrete fourier transform to decompose the successive frames of the signal observed by the SU, we represent the narrowband discrete frequency components as:

$$R_k(m) = H_k S_k(m) + V_k(m),\ k = 0, 1, \ldots, K-1 \tag{4.1}$$

where k is the frequency and m is the frame index. H_k, $S_k(m)$ and $V_k(m)$ denote the k-th DFT coefficients of the subband impulse reponse, $h(n)$; the EU signal, $s(mK+n)$; and the additive white noise, $v(mK+n)$, respectively. Under hypothesis $\mathcal{H}_{0,k}$, the k-th subband is unoccupied and we set $E[|S_k(m)|^2] = 0$, while, under hypothesis $\mathcal{H}_{1,k}$, an EU is present in the k-th subband and we set $E[|S_k(m)|^2] = 1$. The EU signal samples, $\{S_k(m)\}$, and noise samples, $\{V_k(m)\}$, are modelled as independent random processes, whose samples are assumed to be independent across frequency and frame indices under each hypothesis and to obey a zero-mean complex circular symmetric Gaussian distribution. The noise variance, $\sigma_v^2 \triangleq E[|V_k(m)|^2]$, and the channel squared magnitude response, $G_k \triangleq |H_k|^2$, are assumed to be known from *a priori* estimation.

The measured energy in each subband is denoted as Y_k, which is given by:

$$Y_k \triangleq \sum_{m=1}^{M} |R_k(m)|^2 \tag{4.2}$$

In [12], Y_k is used as the test statistic for the hypothesis test in the k-th subband. This leads to an independent hypothesis test for each of the K subbands. As shown in Section 3.2.2, this is indeed optimum when the subband occupancies are independent of each other. However, in the general case where correlation exists between subband occupancy, the OLEC detector is expected to outperform such decoupled detector structures. Consequently, the SU formulates the following

hypothesis test to perform detection in the k-th subband:

$$Z_k = \boldsymbol{\xi}_k^{oT} \boldsymbol{Y} \underset{\mathcal{H}_{0,k}}{\overset{\mathcal{H}_{1,k}}{\gtrless}} \gamma_k, \quad k = 0, 1, \ldots, K-1 \tag{4.3}$$

where $\boldsymbol{\xi}_k^o$ is the weight vector of the linear combiner for the k-th subband.

In Section 3.3.2, the performance of the OLEC detector is analyzed in terms of the probabilities of false alarm and missed detection. Here, we consider a multiband joint detection framework where we seek the optimum use of the unoccupied spectrum without introducing undesirable interference to the EU systems. In order to achieve this, we quantify the net spectrum use and the net interference addition using two global metrics.

Given (3.32), (3.33) and (4.3), we construct vectors of the detection thresholds used in each of the K subbands and the associated probabilities of false alarm and missed detection for K subbands:

$$\boldsymbol{\gamma} \equiv [\gamma_0, \gamma_1, \ldots, \gamma_{K-1}]^T \tag{4.4}$$

$$\mathbf{P}_f(\boldsymbol{\gamma}) \equiv [P_f^{(0)}(\gamma_0), P_f^{(1)}(\gamma_1), \ldots, P_f^{(K-1)}(\gamma_{K-1})]^T \tag{4.5}$$

$$\mathbf{P}_m(\boldsymbol{\gamma}) \equiv [P_m^{(0)}(\gamma_0), P_m^{(1)}(\gamma_1), \ldots, P_m^{(K-1)}(\gamma_{K-1})]^T \tag{4.6}$$

Consequently, as discussed in Section 2.2.1, if $\boldsymbol{r} \equiv [r_0, r_1, \ldots, r_{K-1}]^T$ denotes the Shannon theoretic capacity for the K subbands, the *aggregate opportunistic throughput* of the SU can be defined as:

$$R(\boldsymbol{\gamma}) \triangleq \boldsymbol{r}^T [\mathbf{1} - \boldsymbol{P}_f(\boldsymbol{\gamma})] \tag{4.7}$$

Similarly, if $\boldsymbol{c} \triangleq [c_0, c_1, \ldots, c_{K-1}]^T$ represents the costs associated with interfering with the EUs in the K subbands, the *aggregate interference* added by the SU (to all the EUs) can be defined

as:

$$C(\boldsymbol{\gamma}) \triangleq \boldsymbol{c}^T \boldsymbol{P}_m(\boldsymbol{\gamma}) \tag{4.8}$$

Given these global metrics of performance, we seek an optimal set of detection thresholds $\{\gamma_k\}_{k=0}^{K-1}$ such that one of the following is achieved:

- Maximize the aggregate opportunistic throughput given an upper bound on the aggregate interference, i.e.:

$$\max_{\boldsymbol{\gamma}} \quad R(\boldsymbol{\gamma}) \tag{4.9a}$$

$$\text{s.t.} \quad C(\boldsymbol{\gamma}) \leq \epsilon \tag{4.9b}$$

$$\boldsymbol{P}_m(\boldsymbol{\gamma}) \leq \boldsymbol{\alpha} \tag{4.9c}$$

$$\boldsymbol{P}_f(\boldsymbol{\gamma}) \leq \boldsymbol{\beta} \tag{4.9d}$$

- Minimize the aggregate interference given a lower bound on the aggregate opportunistic throughput, i.e.:

$$\min_{\boldsymbol{\gamma}} \quad C(\boldsymbol{\gamma}) \tag{4.10a}$$

$$\text{s.t.} \quad R(\boldsymbol{\gamma}) \geq \delta \tag{4.10b}$$

$$\boldsymbol{P}_m(\boldsymbol{\gamma}) \leq \boldsymbol{\alpha} \tag{4.10c}$$

$$\boldsymbol{P}_f(\boldsymbol{\gamma}) \leq \boldsymbol{\beta} \tag{4.10d}$$

As can be seen, the resulting optimization problems are identical to those in (2.33) and (2.34) in Section 2.2.1 except that, now, $P_f^{(k)}$ and $P_m^{(k)}$ are as defined in (3.32) and (3.33) respectively.

In order to bring these problems into tractable forms, we first exploit the monotonicity of the

Q-function to transform (4.9c)-(4.9d) into a linear constraint on the feasible set. The result of this transformation is:

$$\gamma_{min,k} \leq \gamma_k \leq \gamma_{max,k} \tag{4.11}$$

with:

$$\gamma_{min,k} \triangleq E[Z_k|B_k = 0] + Q^{-1}(\beta_k)\sqrt{Var[Z_k|B_k = 0]} \tag{4.12}$$

$$\gamma_{max,k} \triangleq E[Z_k|B_k = 1] + Q^{-1}(1 - \alpha_k)\sqrt{Var[Z_k|B_k = 1]} \tag{4.13}$$

where the moments of Z_k are available from our developments in Section 3.3.2.

As in Section 2.2, in general, the resulting objective and constraint functions are not convex. Hence, neither the existence nor the computability of a solution is guaranteed. However, it can be shown that (4.9) and (4.10) are convex if the parameters α_k and β_k are restricted to $[0, \frac{1}{2}]$. Under these practical restrictions, the multiband joint optimization problems may be simplified to:

- Maximization of the aggregate opportunistic throughput with constraint on the aggregate interference:

$$\begin{aligned} \max_{\boldsymbol{\gamma}} \quad & R(\boldsymbol{\gamma}) \\ \text{s.t.} \quad & \boldsymbol{c}^T \boldsymbol{P}_m(\boldsymbol{\gamma}) \leq \epsilon \\ & \gamma_{min,k} \leq \gamma_k \leq \gamma_{max,k} \end{aligned} \tag{4.14}$$

- Minimization of the aggregate interference with constraint on the aggregate opportunistic

throughput:

$$\begin{aligned} \min_{\boldsymbol{\gamma}} \quad & C(\boldsymbol{\gamma}) \\ \text{s.t.} \quad & \boldsymbol{r}^T[\mathbf{1} - \boldsymbol{P}_f(\boldsymbol{\gamma})] \geq \delta \\ & \gamma_{min,k} \leq \gamma_k \leq \gamma_{max,k} \end{aligned} \tag{4.15}$$

The above inequality-constrained convex optimizations may be solved using any well-known technique such as the interior point or Lagrange-Newton method. In particular, the MATLAB routine `fmincon` provides implementations of several constrained minimization algorithms which may be applied here. In Section 5.2.1, we present numerical results for single-user multiband joint detection to show that the use of the OLEC detector offers significant performance improvements over the use of the traditional decoupled energy detectors. In order to obtain these results, we used MATLAB's implementation of the active set algorithm to solve the optimization problems since it is expected to achieve faster convergence than the other options available in `fmincon`.

4.2 Collaborative Multiband Joint Detection

The single-user detection schemes, such as the one considered in Section 4.1, are susceptible to blockage effects, such as shadowing or multipath fading, that negatively impact the sensing performance. Current literature advocates the use of multi-user collaboration in order to overcome these effects. For example, [2], [13] and [14], discuss distributed sensing using linear cooperation. Here, we study the performance improvement obtained through the use of the OLEC detector in the multi-user detection framework discussed in Section 2.2.2 when subband occupancies are correlated. This development is analogous to the single-user counterpart described above in Section 4.1.

4.2.1 Optimum Linear Energy Combiner for Collaborative Detection

Consider N SUs (i.e., CR units) that collaborate to detect the presence of EU signals in K subbands. As in the single-user case, following a K-point discrete fourier transform to decompose the signal frames observed by each SU, the narrowband frequency component observed by the n-th SU can be written as:

$$R_k^n(m) = H_k^n S_k(m) + V_k^n(m) \quad \begin{cases} k = 0, 1, \ldots, K-1 \\ m = 0, 1, \ldots, M-1 \\ n = 0, 1, \ldots, N-1 \end{cases} \tag{4.16}$$

where k is the frequency index and m is the frame index. H_k^n denotes the k-th DFT coefficient of the subband impulse response between the EU and the n-th SU, and $G_k^n = |H_k^n|^2$ denotes its square magnitude. $R_k^n(m)$ and $V_k^n(m)$ respectively denote the k-th DFT coefficients of the received signal and the white noise observed by n-th SU during the m-th frame. The squared channel magnitudes, G_k^n, and the noise variance, σ_v^2, are expected to be known from *a priori* estimation.

The same EU signal, $S_k(m)$, is observed by all the SUs. Under $\mathcal{H}_{0,k}$, we set $E[|S_k(m)|^2] = 0$, indicating an absence of EU signal, while, under $\mathcal{H}_{1,k}$, we set $E[|S_k(m)|^2] = 1$, indicating a presence of EU signal. Under each hypothesis, samples of $\{S_k(m)\}$ and $\{V_k^n(m)\}$ are assumed to be independent across time, frequency, and SU indices and to follow zero-mean circular symmetric Gaussian distribution. We model the occupancy of the k-th subband using the binary random variable, B_k, with realization $b_k \in \{0, 1\}$, where 0 and 1 correspond to $\mathcal{H}_{0,k}$ and $\mathcal{H}_{1,k}$ respectively. It follows that $E[|S_k(m)|^2 \big| B_k = b_k] = b_k$.

The n-th SU measures the energy in the k-th subband as follows:

$$Y_k^n = \sum_{m=0}^{M-1} |R_k^n(m)|^2 \tag{4.17}$$

Detection is carried out at the so-called fusion centre, which may be one of the collaborating SUs (e.g., the 0^{th} SU) or a network entity (e.g., a base station), based on the observations made by these N spatially distributed SUs. The fusion centre takes a decision about the occupancy of the k-th subband based on the energy measurements from the N SUs, which we represent by the following $N \times 1$ vector:

$$\boldsymbol{Y}_k \equiv [Y_k^0, Y_k^1, \ldots, Y_k^{N-1}]^T \tag{4.18}$$

Although a few different fusion schemes have been proposed in the literature for generating test statistics from measurements made at multiple spatially dispersed SUs, here, we consider the linear weighing scheme discussed in [12]:

$$U_k = \sum_{n=0}^{N-1} w_k^n Y_k^n = \boldsymbol{w}_k^T \boldsymbol{Y}_k \tag{4.19}$$

where $\boldsymbol{w}_k = [w_k^0, w_k^1, \ldots, w_k^{N-1}]^T$ are the weights used to combine the N energy measurements for the k-th subband. The weight values used for all the subbands can be compactly denoted as:

$$W = [\boldsymbol{w}_0, \boldsymbol{w}_1, \ldots, \boldsymbol{w}_{K-1}] = \begin{bmatrix} w_0^0 & w_1^0 & \cdots & w_{K-1}^0 \\ w_0^1 & w_1^1 & \cdots & w_{K-1}^1 \\ \vdots & \vdots & \ddots & \vdots \\ w_0^{N-1} & w_1^{N-1} & \cdots & w_{K-1}^{N-1} \end{bmatrix} \tag{4.20}$$

Given such a fusion scheme, our objective is to develop a multi-user counterpart of the single-

user OLEC detector described in Section 3.3. That is, we seek to detect the k-th subband's occupancy, as represented by B_k, through a single hypothesis test on a statistic generated by linearly combining the energy measurements, $\{U_k\}_{k=0}^{K-1}$. Consequently, we define $\hat{B}_k$, the estimate of the occupancy of the k-th subband, as an affine transformation on the energy vector $\boldsymbol{U} = [U_0, U_1, \ldots, U_{K-1}]^T$:

$$\hat{B}_k = \boldsymbol{\xi}_k^T \boldsymbol{U} + \epsilon_k \tag{4.21}$$

As in the single-user detection case, the weight vector $\boldsymbol{\xi}_k$ and the constant ϵ_k are obtained as the minimizer of the MSE:

$$J(\boldsymbol{\xi}_k, \epsilon_k) = E[(\hat{B}_k - B_k)^2] \tag{4.22}$$

$$= E[(\boldsymbol{\xi}_k^T \boldsymbol{U} + \epsilon_k - B_k)^2] \tag{4.23}$$

As before, by defining the centred quantities $\tilde{\boldsymbol{U}} = \boldsymbol{U} - E[\boldsymbol{U}]$ and $\tilde{B}_k = B_k - \mu_k$, where $\mu_k = E[B_k]$, the MMSE weight vector can be shown to be[1]:

$$\boldsymbol{\xi}_k^o = E[\tilde{\boldsymbol{U}}\tilde{\boldsymbol{U}}^T]^{-1} E[\tilde{\boldsymbol{U}}\tilde{B}_k] \tag{4.24}$$

Since B_k has a non-zero mean, the optimum value of the bias term ϵ_k is necessary and it can be shown to be $\epsilon_k^o = \mu_k - \boldsymbol{\xi}_k^{oT} E[\boldsymbol{U}]$, where $E[U_i] = \boldsymbol{w}_i^T E[\boldsymbol{Y}_i]$. Using (4.19), we can write:

$$E[\tilde{U}_i \tilde{B}_k] = \boldsymbol{w}_i^T E[\tilde{\boldsymbol{Y}}_i \tilde{B}_k] \tag{4.25}$$

$$E[\tilde{U}_i \tilde{U}_j] = \boldsymbol{w}_i^T E[\tilde{\boldsymbol{Y}}_i \tilde{\boldsymbol{Y}}_j^T] \boldsymbol{w}_j^T \tag{4.26}$$

where we define the centred quantity, $\tilde{\boldsymbol{Y}}_k = \boldsymbol{Y}_k - E[\boldsymbol{Y}_k]$. By substituting (4.16) into (4.17), we

[1] Further details can be found in Appendix A.

can further show that:

$$E[\tilde{Y}_i^n \tilde{B}_k] = M(\lambda_{ik} - \mu_i\mu_k)G_i^n \tag{4.27}$$

$$E[\tilde{Y}_i^n \tilde{Y}_j^{n'}] = M^2(\lambda_{ij} - \mu_i\mu_j)G_i^n G_j^{n'} + M(\mu_i G_i^n G_i^{n'} + 2\mu_i G_i^n \sigma_v^2 \delta_{nn'} + \sigma_v^4 \delta_{nn'})\delta_{ij} \tag{4.28}$$

where $\lambda_{ij} = E[B_i B_j]$ as defined in Section 3.1. From (4.28), it should be noted that, in constrast to the treatment shown in [7], the matrix $E[\boldsymbol{Y}_k \boldsymbol{Y}_k^T]$ is not diagonal in general.

The resulting detector for the k-th subband can be written as:

$$Z_k = \boldsymbol{\xi}_k^{oT} \boldsymbol{U} \underset{\mathcal{H}_{0,k}}{\overset{\mathcal{H}_{1,k}}{\gtrless}} \gamma_k, \quad k = 0, 1, \ldots, K-1 \tag{4.29}$$

It should be noted that the bias term ϵ_k^o is absorbed in the detection threshold γ_k and $\boldsymbol{\xi}_k^o$ can be normalized such that $\xi_{kk}^o = 1$.

4.2.2 Performance of OLEC-based Collaborative Detection

The minimum attainable probability of missed detection for a given upper limit on the probability of false alarm provides an objective measure of the detection performance. Hence, we compute these probabilities for the multi-user OLEC detector developed here. Conditioned on $B_k = b_k$, the mean and variance of the test statistic, Z_k, in (4.29) can be written as[2]:

$$E[Z_k | B_k = b_k] = \boldsymbol{\xi}_k^{oT} E[\boldsymbol{U} | B_k = b_k] \tag{4.30}$$

$$\mathit{Var}[Z_k | B_k = b_k] = \boldsymbol{\xi}_k^{oT} E[\tilde{\boldsymbol{U}} \tilde{\boldsymbol{U}}^T | B_k = b_k] \boldsymbol{\xi}_k^o \tag{4.31}$$

[2]Further details can be found in Appendix B.

Using the definition of U_k in (4.19), we can show:

$$E[U_i|B_k = b_k] = \boldsymbol{w}_i^T E[\mathbf{Y}_i|B_k = b_k] \tag{4.32}$$

$$E[\tilde{U}_i\tilde{U}_j|B_k = b_k] = \boldsymbol{w}_i^T E[\tilde{\mathbf{Y}}_i\tilde{\mathbf{Y}}_j^T|B_k = b_k]\boldsymbol{w}_j^T \tag{4.33}$$

Evaluation of the expected values of the right-hand sides of (4.32) and (4.33) yields:

$$E[Y_i^n|B_k = b_k] = M(G_i^n\mu_{i|k} + \sigma_v^2) \tag{4.34}$$

$$E[\tilde{Y}_i^n\tilde{Y}_j^{n'}|B_k = b_k] = M^2G_i^nG_j^{n'}(\lambda_{ij|k} - \mu_{i|k}\mu_{j|k}) + M[\mu_{i|k}G_i^nG_i^{n'} + 2\mu_{i|k}G_i^n\sigma_v^2\delta_{nn'} + \sigma_v^4\delta_{nn'}]\delta_{ij} \tag{4.35}$$

where $\mu_{i|k} = E[B_i|B_k = b_k]$ and $\lambda_{ij|k} = E[B_iB_j|B_k = b_k]$ as defined in Section 3.3.2.

According to the central limit theorem, for a sufficiently large M, U_k and, hence, in turn, Z_k can be assumed to be normally distributed under both $\mathcal{H}_0$ and $\mathcal{H}_1$. Consequently, the probabilities of false alarm and missed detection associated with (4.29) are given by:

$$P_f^{(k)}(W, \gamma_k) = Q\left(\frac{\gamma_k - E[Z_k|B_k = 0]}{\sqrt{Var[Z_k|B_k = 0]}}\right) \tag{4.36}$$

$$P_m^{(k)}(W, \gamma_k) = 1 - Q\left(\frac{\gamma_k - E[Z_k|B_k = 1]}{\sqrt{Var[Z_k|B_k = 1]}}\right) \tag{4.37}$$

4.2.3 Spatial-Spectral Joint Detection Using the OLEC

In order to attain the optimal use of the spectrum holes without adding undesirabele levels of interference to the EUs, we need quantifiable measures of the net spectrum usage and net interference addition to EUs. Hence, in a similar fashion to the single-user multiband joint detection

scenario, using (4.29), (4.36) and (4.37), we construct the following vectors:

$$\boldsymbol{\gamma} \equiv [\gamma_0, \gamma_1, \ldots, \gamma_{K-1}]^T \tag{4.38}$$

$$\mathbf{P}_f(W, \boldsymbol{\gamma}) \equiv [P_f^{(0)}(W, \gamma_0), P_f^{(1)}(W, \gamma_1), \ldots, P_f^{(K-1)}(W, \gamma_{K-1})]^T \tag{4.39}$$

$$\mathbf{P}_m(W, \boldsymbol{\gamma}) \equiv [P_m^{(0)}(W, \gamma_0), P_m^{(1)}(W, \gamma_1), \ldots, P_m^{(K-1)}(W, \gamma_{K-1})]^T \tag{4.40}$$

As in Section 2.2.2, in this formulation the dependence on the weight matrix has been made explicit. Using these notations, the *aggregate opportunistic throughput* and the *aggregate interference* can be defined as perfomance metrics for the multi-user case as follows:

$$R(W, \boldsymbol{\gamma}) \triangleq \boldsymbol{r}^T[\mathbf{1} - \boldsymbol{P}_f(W, \boldsymbol{\gamma})] \tag{4.41}$$

$$C(W, \boldsymbol{\gamma}) \triangleq \boldsymbol{c}^T \boldsymbol{P}_m(W, \boldsymbol{\gamma}) \tag{4.42}$$

where $\boldsymbol{c} \triangleq [c_0, c_1, \ldots, c_{K-1}]^T$ represents the costs associated with interfering with the primary users in the K subbands, and $\boldsymbol{r} \equiv [r_0, r_1, \ldots, r_{K-1}]^T$ denotes the Shannon theoretic capacity for the K subbands.

Given these performance metrics, we seek an optimum set of detection thresholds, $\{\gamma_k\}_{k=0}^{K-1}$, and an optimum set of fusion weights, $\{\boldsymbol{w}_k\}_{k=0}^{K=1}$, that achieve one of the following:

- Maximize the aggregate opportunistic throughput given an upper bound on the aggregate interference
- Minimize the aggregate interference given a lower bound on the aggregate opportunistic throughput

The resulting optimization problems are similar to those in (4.9) and (4.10) except for the additional dependence on W. In [12], a sequential optimization procedure is described whereby the

weight coefficients, W, are chosen to maximize the signal-to-noise ratio. This same method is adopted in our work. The optimal weight coefficient for the k-th subband is given by:

$$\boldsymbol{w}_k^o = \frac{\Sigma_k^{-1}\boldsymbol{G}_k}{\|\Sigma_k^{-1}\boldsymbol{G}_k\|_2} \tag{4.43}$$

where $\boldsymbol{G}_k = [G_k^0, G_k^1, \ldots, G_k^{N-1}]$ is the vector of the channel squared magnitude responses between the EU and the N collaborating SUs in the k-th subband, and matrix $\Sigma_k = E[\tilde{\boldsymbol{Y}}_k\tilde{\boldsymbol{Y}}_k^T \big| B_k = 1]$.

The monotonicity of the Q-function can be exploited to transform (4.9c)-(4.9d) into the following linear constraint on the feasible set:

$$\gamma_{min,k} \leq \gamma_k \leq \gamma_{max,k} \tag{4.44}$$

with:

$$\gamma_{min,k} \triangleq E[Z_k|B_k = 0] + Q^{-1}(\beta_k)\sqrt{Var[Z_k|B_k = 0]} \tag{4.45}$$

$$\gamma_{max,k} \triangleq E[Z_k|B_k = 1] + Q^{-1}(1-\alpha_k)\sqrt{Var[Z_k|B_k = 1]} \tag{4.46}$$

The moments of Z_k in (4.45) and (4.46) are as found in Section 4.2.2.

The resulting objective and constraint functions are not generally convex. However, restricting the parameters α_k and β_k to $[0, \frac{1}{2}]$ ensures the optimization problems are convex. Hence, the spatial-spectral problems may be simplified as:

- Maximization of the aggregate opportunistic throughput with constraint on the aggregate

interference:

$$\begin{aligned} \max_{\boldsymbol{\gamma}} \quad & R(W^o, \boldsymbol{\gamma}) \\ \text{s.t.} \quad & \boldsymbol{c}^T \boldsymbol{P}_m(\boldsymbol{\gamma}) \leq \epsilon \\ & \gamma_{min,k} \leq \gamma_k \leq \gamma_{max,k} \end{aligned} \tag{4.47}$$

- Minimization of the aggregate interference with constraint on the aggregate opportunistic throughput:

$$\begin{aligned} \min_{\boldsymbol{\gamma}} \quad & C(W^o, \boldsymbol{\gamma}) \\ \text{s.t.} \quad & \boldsymbol{r}^T [\mathbf{1} - \boldsymbol{P}_f(W^o, \boldsymbol{\gamma})] \geq \delta \\ & \gamma_{min,k} \leq \gamma_k \leq \gamma_{max,k} \end{aligned} \tag{4.48}$$

As in the single-user detection case, the inequality-constrained convex optimizations for the multi-user detection case above may be solved using the MATLAB routine `fmincon`, which provides implementations of several constrained minimization algorithms. In Section 5.2.2, we present numerical results for collaborative multiband joint detection to show that the use of the OLEC detector offers significant performance improvements over the use of the traditional decoupled energy detectors. In order to obtain these results, we used MATLAB's implementation of the active set algorithm to solve the optimization problems since it is expected to achieve faster convergence than the other options available in `fmincon`.

Chapter 5

Numerical Results

In Section 3.3 of this thesis, the optimum linear energy combiner (OLEC) was developed to exploit *a priori* knowledge of correlation between subband occupancy to enhance spectrum sensing performance. In addition to the structure of the OLEC detector, we presented a performance analysis of the detection scheme. In Section 4.1, we studied the theoretical performance of a single-user multiband joint detection scheme when used in conjunction with the OLEC detector; and, in Section 4.2, we extended the use of the OLEC detector to spatial-spectral joint detection. Here, we look at suitable experiments to corroborate the analysis with numerical results.

First, we present the receiver operating characteristic (ROC) curves for the hypothesis test (3.24). We also study the level of performance gain as correlation between subbands varies. Then, experimental results are shown for the single-user multiband joint detection case. Finally, test results for the multi-user joint detection framework are presented.

5.1 Simulations for OLEC Performance

In this section, we first look at Monte Carlo simulations to support the developments in Section 3.3. In these simulations, instances of the random occupancy vector $\boldsymbol{B}$ are generated using a homogeneous Markov chain defined over the discrete frequency index k. The initial state of the chain, B_0, is set to 1 with probability $P_{B_0}(1) \equiv 0.5$, while the states at frequencies $k = 1, \ldots, K-1$ are generated by means of a binary symmetric transition model with parameter p denoting the probability of a change in occupancy, that is:

$$P_{B_{k+1}|B_k}(1|0) = P_{B_{k+1}|B_k}(0|1) = p \tag{5.1}$$

Use of this model allows the computation of the moments μ_i, $\mu_{i|k}$, λ_{ij} and $\lambda_{ij|k}$ introduced in Section 3.3. In particular, given this model, the correlation coefficient between random variables B_{k+1} and B_k can be calculated exactly as:

$$\rho = 1 - 2p \tag{5.2}$$

The noise samples, $V_k(m)$, and EU signal samples, $S_k(m)$, are independently generated complex circular Gaussian random variables with variances $\sigma_v^2 = 1$ and $E[|S_k(m)|^2] = 1$. For each realization of $\boldsymbol{B}$, M data frames, $\{R_k(m)\}$, are generated as per (3.3). Here, we set $K = 8$, $M = 100$ and use: $\mathbf{G} = [G_0, \ldots, G_7] = [0.39, 0.11, 0.25, 0.10, 0.42, 0.37, 0.20, 0.29]$. For this set of parameters, and focusing our evaluation on subband $k = 2$, the optimum weight vector is found to be as shown in Table 5.1.

In addition to the K-dimensional OLEC, we present the sub-optimal combiner in (3.25): using a simplified 3-dimensional version of the MMSE problem for $k = 2$, i.e., using energy measurements from bands $k = 1$ and $k = 3$ only, we obtain the weight values shown in Table 5.2.

Table 5.1 Optimum Weight Vector for OLEC Detector

p	ρ	$\boldsymbol{\xi}_2^o$
0.20	0.6	$[0.132, 0.217, 1.0, 0.200, 0.120, 0.025, 0.006, 0.002]^T$
0.15	0.7	$[0.203, 0.249, 1.0, 0.227, 0.176, 0.047, 0.013, 0.007]^T$

As is expected from intuition, greater weight is placed on energy measurements from adjacent subbands when the occupancy correlation is higher.

Table 5.2 Optimum Weight Values for Reduced Dimensionality Detector

p	ρ	η_-	η_+
0.20	0.6	0.258	0.243
0.15	0.7	0.311	0.291

Detection is performed on the simulated data samples $\{R_k(m)\}$ using hypothesis tests based on the various choices of test statistics, i.e., Y_k (3.18), $Z_k = \boldsymbol{\xi}_k^{oT}\boldsymbol{Y}_k$ (3.24) and $Z_k^{\pm}$ (3.25). In order to obtain reliable estimates of the probabilities of false alarm and missed detection, 10^5 trials are used for each choice of threshold value.

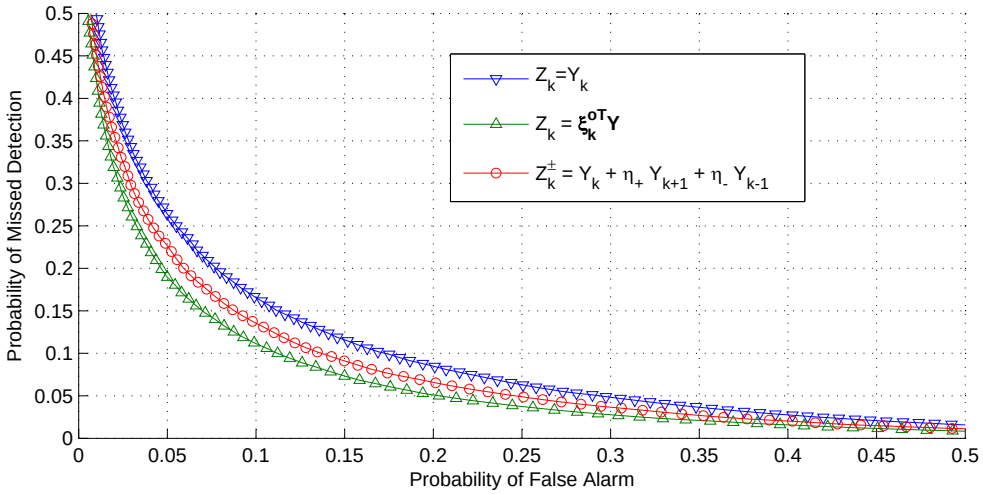

Figure 5.1 $P_m^{(k)}$ versus $P_f^{(k)}$ for $\rho = 0.6$ ($k = 2, p = 0.20$)

Figure 5.1 shows the receiver operating characteristic (ROC) curve of the detectors, obtained by plotting $P_m^{(k)} \equiv P_m^{(k)}(\gamma_k)$ against $P_f^{(k)} \equiv P_f^{(k)}(\gamma_k)$ over a range of threshold parameter values

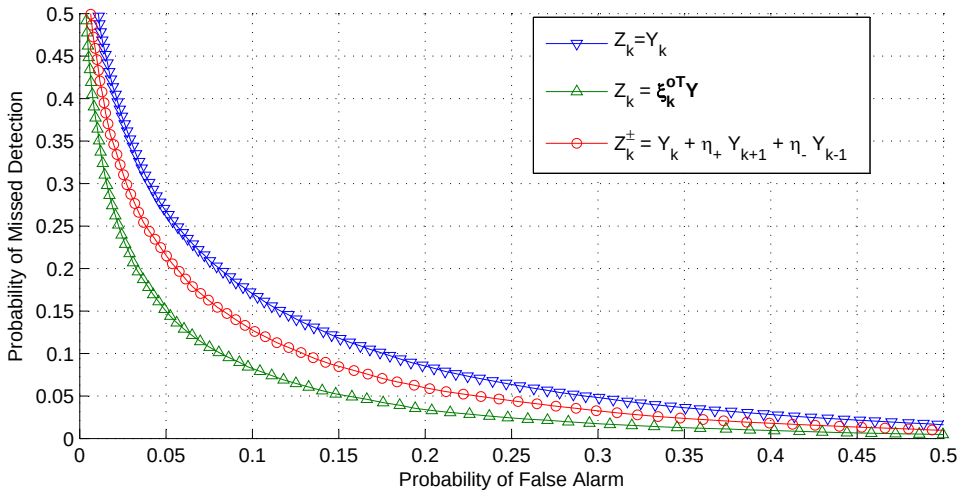

Figure 5.2 $P_m^{(k)}$ versus $P_f^{(k)}$ for $\rho = 0.7$ ($k = 2$, $p = 0.15$)

γ_k, for subband $k = 2$ in the case $p = 0.25$, corresponding to a correlation of $\rho = 0.5$. Figure 5.2 shows the ROC curve for the subband $k = 2$ when $p = 0.15$, or, equivalently, $\rho = 0.7$. Ideally, the operating point should be as close to the origin as possible. For all values of $P_f^{(k)}$, use of the proposed Z_k as a test statistic, instead of the conventional Y_k, significantly reduces $P_m^{(k)}$. In this case, because of the choice of the occupancy probability model, the use of the simplified test statistic $Z_k^{\pm}$ also provides significant improvement, but, in general, its performance may not be as good as that of Z_k. We notice that using Y_k as the test statistic makes the detection performance indifferent to the level of correlation between the subband occupancy. This case represents what we see in contemporary literature, where we assume independent subband occupancy. However, use of Z_k or $Z_k^{\pm}$ allows us to exploit *a priori* knowledge of occupancy correlation and, thereby, improve detection performance.

We note that a bigger performance gain is obtained for $\rho = 0.7$ than for $\rho = 0.6$. This trend seen in Figure 5.1 and Figure 5.2 holds true for other choices of the transition probability p. To illustrate this point, in Figure 5.3, we show the analytically computed probability of missed detection, $P_m^{(k)}$ as a function of the angle $\theta = \arccos(\rho)$ between random variables B_k and B_{k+1}, under the Neyman-Pearson constraint of $P_f^{(k)} = 0.05$. The curves clearly demonstrate the

potential advantages of exploiting *a priori* knowledge of correlation across subband occupancies in the design of a detector structure for spectrum sensing.

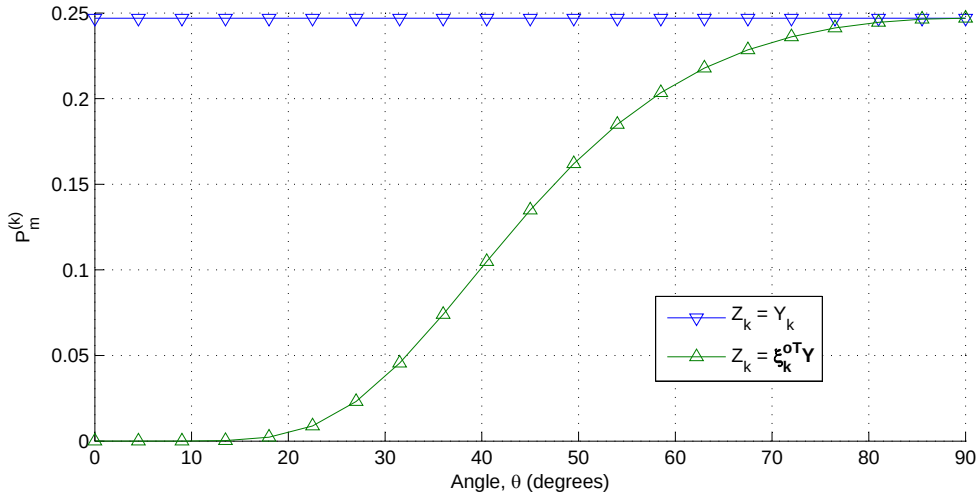

Figure 5.3 $P_m^{(k)}$ versus θ for $P_f^{(k)} = 0.05$ $(k = 2)$

In the following sections, we look at the use of the OLEC detector within the multiband joint detection framework.

5.2 Results for Multiband Joint Detection Using the OLEC

In Section 5.1, we looked at the sensing performance of the OLEC when used to detect the occupancy of a single subband. Here, we will analyze the deployment of OLEC detectors for a multiband system where joint detection is carried out for the occupancy of all the subbands in order to optimise the performance of the overall system through the definition of some global metrics, viz., *aggregate opportunistic throughput* and *aggregate interference*, which are described in detail in Chapter 4.

The results presented in this section are based on the analytically computated values of $P_f(k)$ and $P_m(k)$. This requires the definition of some system parameters as well as a description of the probability model for the occupancy vector $\boldsymbol{B}$. As in Section 5.1, the multiband occupancy

is considered to follow a homogeneous Markov chain defined over the discrete frequency index k. The initial state of the chain, B_0, is set to 1 with probability $P_{B_0}(1) \equiv 0.5$, while the states at frequencies $k = 1, \ldots, K-1$ are generated by means of a binary symmetric transition model with parameter p denoting the probability of a change in occupancy, that is:

$$P_{B_{k+1}|B_k}(1|0) = P_{B_{k+1}|B_k}(0|1) = p \tag{5.3}$$

As before, given this model, the moments μ_i, $\mu_{i|k}$, λ_{ij} and $\lambda_{ij|k}$ introduced in Section 3.3 can be computed.

In addition, the noise variance, $\sigma_v^2 = 1$, and the EU signal variance, $E[|S_k(m)|^2] = 1$. For both the single-user and multi-user detection scenarios, we set the number of subbands, $K = 8$, and the number of data frames, $M = 100$. In the following subsections, we analyze these two cases separately. For these experiments, the minimum opportunistic spectrum use is set to 50%, or, equivalently, $\beta_k = 0.5$. The maximum acceptable probability that the SU interfers with the EU is set to, 20%, or, $\alpha_k = 0.2$.

5.2.1 Results for Single-User Detection

In this numerical evaluation, we compare a (single-user) multiband joint detection scheme using independent band-by-band hypothesis tests to one employing the OLEC to detect the occupancy in every subband based on multiband energy measurements. The former is described in Section 2.2.1, while the latter is described in Section 4.1. The values of the channel squared magnitude, opportunistic rate and interference penalty for each subband are summarized in Table 5.3.

Figure 5.4 plots the maximum aggregate opportunistic throughput attainable against the constraint on the aggregate interference obtained by solving the optimization problem in (4.9) for the case where occupancy correlation between adjacent subbands, B_k and B_{k+1}, is $\rho = 0.7$. It can

Table 5.3 Parameters Used in the Single-User Multiband Joint Detection Experiment

k	0	1	2	3	4	5	6	7
G_k	0.61	0.49	0.35	0.25	0.23	0.35	0.52	0.59
r_k (kbps)	612	524	623	139	451	409	909	401
c_k	1.91	8.17	4.23	3.86	7.16	6.05	0.82	1.30

be seen that the use of the OLEC achieves much higher throughput than does the use of the decoupled detectors. The detector proposed in this thesis is able to exploit the knowledge of correlation to improve spectral utilization for any choice of constraint on the interference.

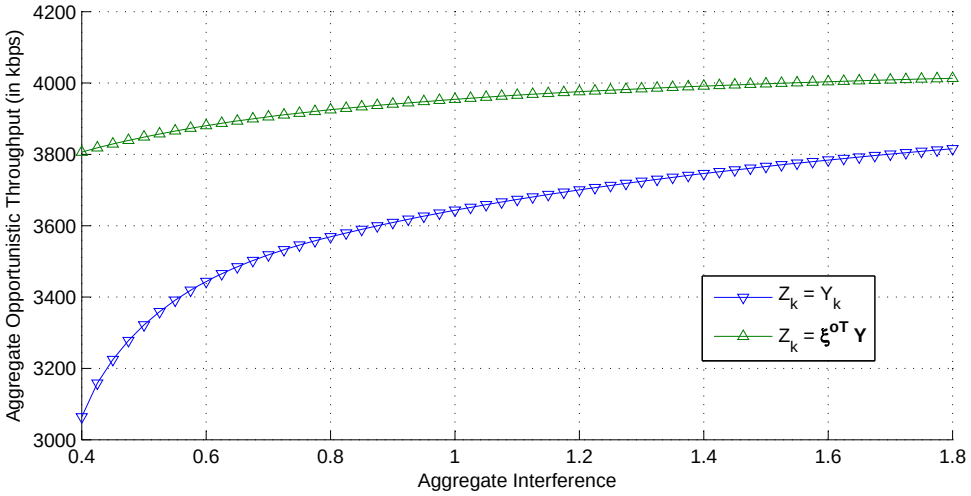

Figure 5.4 The maximum aggregate opportunistic throughput of the SU against the constraint on the aggregate interference to the EU when $\rho = 0.7$ ($p = 0.15$)

In Figure 5.5, we look at the converse problem formulated in (4.10). This figure plots the minimum aggregate interference attainable against the constraint on the aggregate opportunistic throughput. As in the dual problem, we set the occupancy correlation between adjacent subbands, B_k and B_{k+1}, to be $\rho = 0.7$. Similar performance improvements are seen in this case too. For any choice of lower bound on the aggregate opportunistic throughput, the use of the OLEC achieves much lower aggregate interference by exploiting the knowledge of occupancy correlation.

In both cases, we see that the use of *a priori* knowlege of correlation between subband oc-

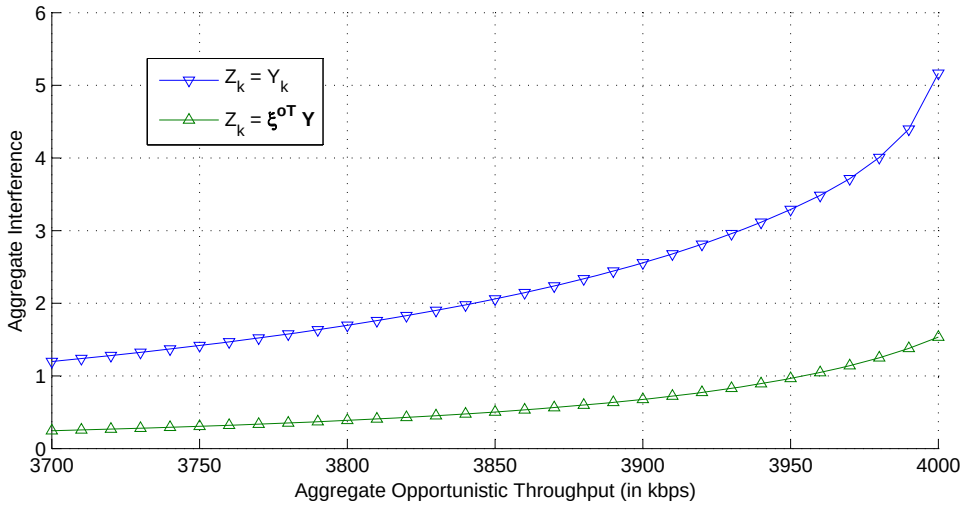

Figure 5.5 The minimum aggregate interference to the EU against the constraint on the aggregate opportunistic throughput of the SU when $\rho = 0.7$ ($p = 0.15$)

cupancy can obtain significant performance gains in multiband joint spectrum sensing tasks. For instance, in the results shown here, the gain in spectral utilization was as high as 25% for an interference limit of 0.4. In the next section, we will study the performance of the OLEC in the multi-user case.

5.2.2 Results for Collaborative Detection

In this section, we present some numerical results for a collaborative multiband joint detection scheme in order to compare the performance of a system using decoupled detection against one using the OLEC detector for each subband. These detection schemes are described in Sections 2.2.2 and 4.2 respectively. Here, we consider a system with two collaborating SUs, i.e., $N = 2$. Table 5.4 shows the values of the channel squared magnitude for the SUs, and the opportunistic rate and interference penalty for each subband.

For this choice of parameters, Figure 5.6 plots the maximum aggregate opportunistic throughput attainable against the constraint on the aggregate interference obtained by solving the optimization problem in (4.47) for the case where occupancy correlation between adjacent subbands, B_k

Table 5.4 Parameters Used in the Collaborative Multiband Joint Detection Experiment

k	0	1	2	3	4	5	6	7
G_k^0	0.38	0.29	0.23	0.26	0.35	0.39	0.33	0.27
G_k^1	0.51	0.40	0.31	0.19	0.21	0.27	0.43	0.50
r_k (kbps)	802	755	356	327	68	720	15	972
c_k	5.95	3.91	0.71	4.21	0.44	2.03	0.58	2.85

and B_{k+1}, is $\rho = 0.7$. It can be seen that the use of the OLEC achieves much higher throughput than does the use of the decoupled detectors.

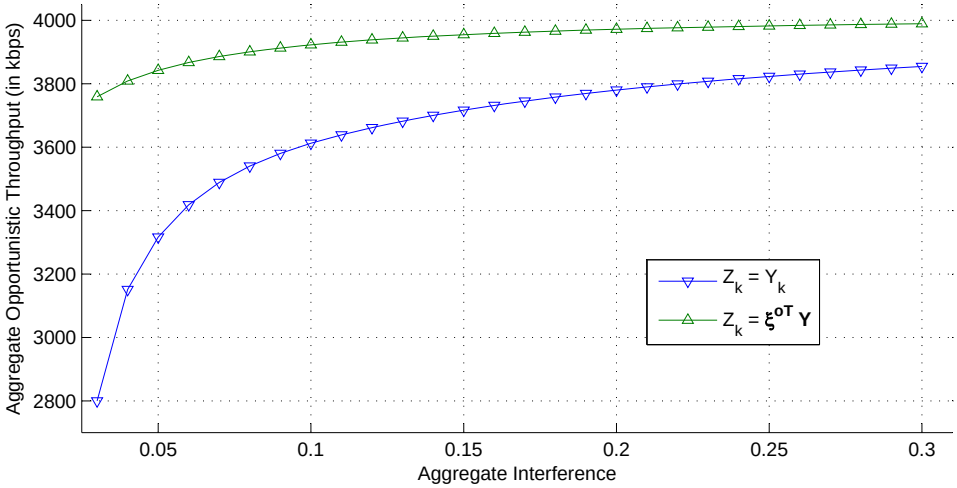

Figure 5.6 The maximum aggregate opportunistic throughput of the SUs against the constraint on the aggregate interference to the EU when $\rho = 0.7$ ($p = 0.15$)

In Figure 5.7, we look at the solutions to the dual problem formulated in (4.48). This figure plots the minimum aggregate interference attainable against the constraint on the aggregate opportunistic throughput. As in the above problem, we set the occupancy correlation between adjacent subbands, B_k and B_{k+1}, to be $\rho = 0.7$. We notice similar performance improvements here as well. For any choice of lower bound on the aggregate opportunistic throughput, the use of the OLEC achieves much lower aggregate interference by exploiting the knowledge of subband occupancy correlation.

The results in this section demonstrate the advantage of using the OLEC detector when sub-

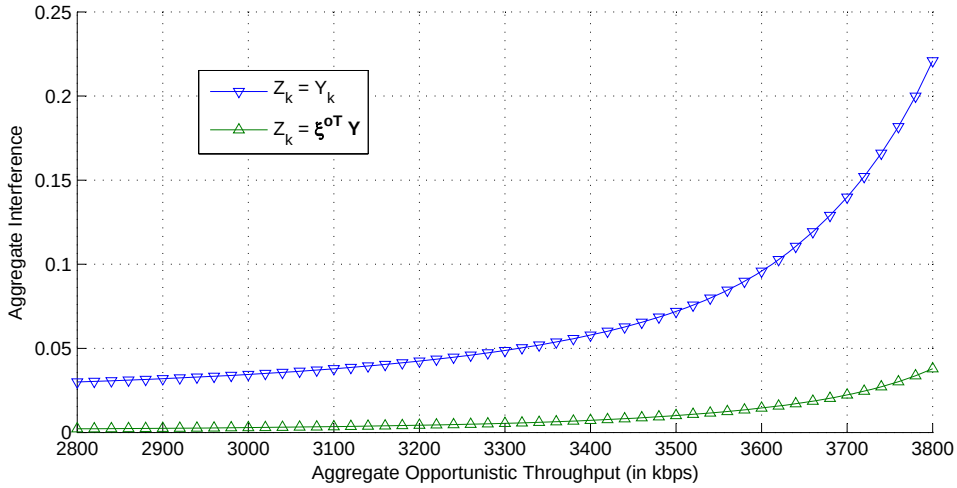

Figure 5.7 The minimum aggregate interference to the EU against the constraint on the aggregate opportunistic throughput of the SUs when $\rho = 0.7$ ($p = 0.15$)

band occupancies are correlated. Compared to the decoupled detector, the OLEC attains much better spectral utilization for any given interference limit. This not only applies to the detection task for a single subband, but also extends to (single-user) multiband joint detection as well as multi-user collaborative detection. Through numerical results, we were able to establish the superior sensing performance of the OLEC detector compared to the traditional decoupled detector contemporarily being used for cognitive radio applications.

Chapter 6

Conclusion

This thesis considered the problem of wideband spectrum sensing for cognitive radio applications. In particular, we considered the sensing task in scenarios where there exists a correlation between subband occupancy. The goal was to exploit *a priori* knowledge of such correlation to improve detection performance. In this section, we summarize the various detector structures presented in this thesis and we also suggest some directions that may be considered for furthur work in this area.

6.1 Thesis Summary

The thesis began with an overview of spectrum sensing in the context of cognitive radios. To this end, some of the techniques currently in use were presented. We broadly classified the sensing schemes under feature detection and energy detection. We discussed how feature detection techniques, such as the use of cyclostationarity properties and matched filtering, are heavily reliant on prior knowledge of the EU signal. This drawback renders such techniques less useful in the context of wideband occupancy detection. We then proceeded to discuss energy detection, which

has found widespread use in literature owing to its flexibility and robustness. Energy detector's performance can be further enhanced by multi-user collaboration in the detection task. Examples of both single-user and multi-user collaborative detection shemes were presented in Section 2.2. As was seen, even in sophisticated contemporary work, it is assumed that subband occupancies are independent of each other, when in reality, due to the presence of wideband PU/EU signals, e.g., WLAN or broadcast television [31], such assumptions are generally not accurate.

In practice, subband occupancy is expected to exhibit various degrees of correlation owing to the spectral allocation plan and to the presence of wideband PU/EU signals. Hence, by suitably modelling the wideband channel occupancy through the use of a random indicator vector, we sought an efficient detector of spectrum holes that could exploit *a priori* knowledge of correlation in occupancy for better sensing performance. We formulated a MAP estimator of this wideband channel occupancy vector. Although the MAP estimator produces computationally tractable detectors in the special case of independent subband occupancy, in the general case of correlated subband occupancy, its complexity grows exponentially with the number of subbands. We therefore proposed an alternative multiband detection structure, the optimum linear energy combiner (OLEC). In this scheme, energy measurements from multiple subbands are linearly combined, using weights derived through a minimum mean-square (MMSE) error criterion, to form a statistic on which a binary hypothesis test can be run to detect the occupancy of any subband. A simpler reduced dimensionality version of the OLEC was also presented along with a detailed performance analysis of the general OLEC detector. In Section 5.1, through numerical simulations, we showed that indeed the OLEC detector outperforms the traditional decoupled detectors in the presence of correlated subband occupancy.

Finally, we looked at the deployment of the OLEC detector in multiband joint detection schemes, e.g., [12] — both in single-user and multi-user frameworks. Instead of optimizing the detector performance in the Neyman-Pearson sense, we considered definition of global metrics,

aggregate opportunistic throughput and *aggregate interference*, to seek optimal spectrum usage for the overall wideband system given a global interference limit. We presented the overall detector structures as well as detailed performance analyses of the detectors. In Section 5.2, we used numerical test results to show that the use of OLEC detector significantly improves the detection performance of both the multiband joint detection and the collaborative multiband detection (spatial-spectral joint detection) schemes.

6.2 Future Research Directions

This thesis showed ways to exploit *a priori* knowledge of correlation between subband occupancy in order to improve wideband channel sensing performance. However, there is scope for furthur improvement to channel sensing techniques in the cognitive radio context. Some examples include:

- In a similar fashion to the development of the OLEC detector in thesis, it is possible to create a multi-user detection framework where energy measurements from multiple users as well as multiple subbands is combined by the OLEC to make decisions in each subband. This should create a simpler multi-user detector structure where only a single layer of combination of energy measurements is used. The performance is also likely to be better.

- The formalism used in this thesis opens the door to incorporation of ideas from the field of digital communications (e.g., multi-user detection and decision feedback) in order to obtain a more flexible trade-off between complexity and performance of wideband channel sensing.

- It may be possible to optimize the number of observation samples used to make decisions as a function of the signal-to-noise ratio in a particular subband. Some overview of such

optimization can be found in [7]. This approach would seem attractive for time-varying applications or it could make the sensing task faster.

Appendix A

Derivation of OLEC Weights

In this appendix, we derive (3.21). Using (3.17) and (3.19), we can write the MSE as:

$$J(\boldsymbol{\xi}_k, \epsilon_k) = \boldsymbol{\xi}_k^T E[\boldsymbol{Y}\boldsymbol{Y}^T]\boldsymbol{\xi}_k + 2\boldsymbol{\xi}_k^T E[\boldsymbol{Y}(\epsilon_k - B_k)] + E[(\epsilon_k - B_k)^2] \tag{A.1}$$

First, we can minimize the MSE with respect to the scalar parameter ϵ_k as follows:

$$\begin{aligned} \frac{\partial}{\partial \epsilon_k} J(\boldsymbol{\xi}_k, \epsilon_k) &= 2\boldsymbol{\xi}_k^T E[\boldsymbol{Y}] + 2E[(\epsilon_k - B_k)] = 0 \\ \therefore \epsilon_k^o &= E[B_k] - \boldsymbol{\xi}_k^T E[\boldsymbol{Y}] \end{aligned} \tag{A.2}$$

Given the optimum value of ϵ_k^o, the MSE can be re-written as follows:

$$J(\boldsymbol{\xi}_k) = \boldsymbol{\xi}_k^T E[\tilde{\boldsymbol{Y}}\tilde{\boldsymbol{Y}}^T]\boldsymbol{\xi}_k - 2\boldsymbol{\xi}_k^T E[\tilde{B}_k\tilde{\boldsymbol{Y}}] + E[\tilde{B}_k^2] \tag{A.3}$$

where $\tilde{\boldsymbol{Y}} = \boldsymbol{Y} - E[\boldsymbol{Y}]$ and $\tilde{B}_k = B_k - E[B_k]$ as described in Section 3.3. Consequently, the MSE can be minimized with respect to $\boldsymbol{\xi}_k$ as follows:

$$\begin{aligned} \frac{\partial}{\partial \boldsymbol{\xi}_k} J(\boldsymbol{\xi}_k) &= 2E[\tilde{\boldsymbol{Y}}\tilde{\boldsymbol{Y}}^T]\boldsymbol{\xi}_k - 2E[\tilde{B}_k\tilde{\boldsymbol{Y}}] = 0 \\ \therefore \boldsymbol{\xi}_k^o &= E[\tilde{\boldsymbol{Y}}\tilde{\boldsymbol{Y}}^T]^{-1}E[\tilde{B}_k\tilde{\boldsymbol{Y}}] \end{aligned} \tag{A.4}$$

Computation of the moments $E[\boldsymbol{Y}]$, $E[\tilde{\boldsymbol{Y}}\tilde{\boldsymbol{Y}}^T]$ and $E[B_k\tilde{\boldsymbol{Y}}]$ needed to evaluate the optimum solutions, (A.2) and (A.4), can be found in Appendix B.

Appendix B

Derivation of Moments of $\boldsymbol{Y}$

In this appendix, we show the derivation of the $E[\boldsymbol{Y}]$, $E[\boldsymbol{Y}\boldsymbol{Y}^T]$ and $E[B_k\boldsymbol{Y}]$ used in this thesis. Although only the single-user unconditional case is shown here, the multi-user and conditioned versions of the moments can be computed similarly as well.

B.1 Derivation of $E[\boldsymbol{Y}]$

Using the definition of Y_k in (3.18) and of $R_k(m)$ in (3.3), we can proceed as follows:

$$\begin{aligned} E[Y_i] &= E\left[\sum_{m=0}^{M-1} |R_i(m)|^2\right] \\ &= \sum_{m=0}^{M-1} E[(H_iS_i(m) + V_i(m))^*(H_iS_i(m) + V_i(m))] \\ &= \sum_{m=0}^{M-1} E[|H_i|^2|S_i(m)|^2 + H_i^*S_i^*(m)V_i(m) + H_iS_i(m)V_i^*(m) + |V_i(m)|^2] \\ &= M\big(E[B_i]G_i + \sigma_v^2\big). \end{aligned} \tag{B.1}$$

B.2 Derivation of $E[\tilde{B}_k\tilde{\boldsymbol{Y}}]$

We first consider the moment $E[B_kY_i]$. Using (3.18) and (3.3), we can write:

$$\begin{aligned}
E[B_kY_i] &= E\left[B_k\sum_{m=0}^{M-1}|R_i(m)|^2\right] \\
&= \sum_{m=0}^{M-1}E[B_k(H_iS_i(m)+V_i(m))^*(H_iS_i(m)+V_i(m))] \\
&= \sum_{m=0}^{M-1}E[B_k(|H_i|^2|S_i(m)|^2+H_i^*S_i^*(m)V_i(m)+H_iS_i(m)V_i^*(m)+|V_i(m)|^2)] \\
&= M\big(E[B_k|S_i(m)|^2]G_i+E[B_k]\sigma_v^2\big) \qquad \text{(B.2)}
\end{aligned}$$

Now, $E[B_k|S_i(m)|^2]$ may be computed as follows:

$$\begin{aligned}
E[B_k|S_i(m)|^2] &= \sum_{b_0=0}^{1}\cdots\sum_{b_{K-1}=0}^{1}E[B_k|S_i(m)|^2\big|\boldsymbol{B}=\boldsymbol{b}]\Pr(\boldsymbol{B}=\boldsymbol{b}) \\
&= \sum_{b_0=0}^{1}\cdots\sum_{b_{K-1}=0}^{1}b_kb_i\Pr(\boldsymbol{B}=\boldsymbol{b}) \\
&= E[B_kB_i] \qquad \text{(B.3)}
\end{aligned}$$

Consequently,

$$E[B_kY_i] = M\big(E[B_kB_i]G_i+E[B_k]\sigma_v^2\big) \qquad \text{(B.4)}$$

and, finally,

$$\begin{aligned}
E[\tilde{B}_k\tilde{Y}_i] &= E[B_kY_i]-E[B_k]E[Y_i] \\
&= M\big(E[B_kB_i]G_i+E[B_k]\sigma_v^2\big)-M\big(E[B_i]G_i+\sigma_v^2\big)E[B_k] \\
&= M\big(E[B_iB_k]-E[B_i]E[B_k]\big)G_i. \qquad \text{(B.5)}
\end{aligned}$$

B.3 Derivation of $E[\tilde{\boldsymbol{Y}}\tilde{\boldsymbol{Y}}^T]$

First consider the moment $E[Y_iY_j]$. As before, using (3.18) and (3.3), we can write:

$$E[Y_iY_j] = \sum_{m=0}^{M-1}\sum_{m'=0}^{M-1} E\left[|R_i(m)|^2|R_j(m')|^2\right] \tag{B.6}$$

where

$$|R_i(m)|^2 = |H_i|^2|S_i(m)|^2 + H_i^*S_i^*(m)V_i(m) + H_iS_i(m)V_i^*(m) + |V_i(m)|^2 \tag{B.7}$$

$$|R_j(m')|^2 = |H_j|^2|S_j(m')|^2 + H_j^*S_j^*(m')V_j(m') + H_jS_j(m')V_j^*(m') + |V_j(m')|^2 \tag{B.8}$$

$$\therefore E[Y_iY_j] = \sum_{m=0}^{M-1}\sum_{m'=0}^{M-1}\sum_{p=1}^{4}\sum_{q=1}^{4} T_{ij}^{pq} \tag{B.9}$$

where T_{ij}^{pq} refers to the following terms:

$$\begin{aligned} T_{ij}^{11} &= G_iG_jE[|S_i(m)|^2|S_j(m')|^2] \\ &= G_iG_jE[S_i(m)S_i^*(m)S_j(m')S_j^*(m')] \\ &= G_iG_jE[B_iB_j](1+\delta_{ij}\delta_{mm'}) \end{aligned} \tag{B.10}$$

$$T_{ij}^{12} = G_iH_j^*E[|S_i(m)|^2S_j^*(m')V_j(m)] = 0 \tag{B.11}$$

$$T_{ij}^{13} = G_iH_jE[|S_i(m)|^2S_j(m')V_j^*(m')] = 0 \tag{B.12}$$

$$\begin{aligned} T_{ij}^{14} &= G_iE[|S_i(m)|^2|V_j(m')|^2] \\ &= G_i\sigma_v^2E[B_i] \end{aligned} \tag{B.13}$$

$$T_{ij}^{21} = G_jH_i^*E[S_i^*(m)V_i(m)|S_j(m')|^2] = 0 \tag{B.14}$$

$$T_{ij}^{22} = H_i^*H_j^*E[S_i^*(m)V_i(m)S_j^*(m')V_j(m')] = 0 \tag{B.15}$$

$$\begin{aligned} T_{ij}^{23} &= H_i^*H_jE[S_i^*(m)V_i(m)S_j(m')V_j^*(m')] \\ &= G_i\sigma_v^2E[B_i]\delta_{ij}\delta mm' \end{aligned} \tag{B.16}$$

$$T_{ij}^{24} = H_i^*E[S_i^*(m)V_i(m)|V_j(m')|^2] = 0 \tag{B.17}$$

$$T_{ij}^{31} = H_i|H_j|^2E[S_i(m)V_i^*(m)|S_j(m')|^2] = 0 \tag{B.18}$$

$$\begin{aligned} T_{ij}^{32} &= H_iH_j^*E[S_i(m)V_i^*(m)S_j^*(m')V_j(m')] \\ &= G_i\sigma_v^2E[B_i]\delta_{ij}\delta mm' \end{aligned} \tag{B.19}$$

$$T_{ij}^{33} = H_i H_j E[S_i(m)V_i^*(m)S_j(m')V_j^*(m')] = 0 \tag{B.20}$$

$$T_{ij}^{34} = H_i E[S_i(m)V_i^*(m)|V_j(m')|^2] = 0 \tag{B.21}$$

$$\begin{aligned} T_{ij}^{41} &= G_j E[|V_i(m)|^2|S_j(m')|^2] \\ &= G_j \sigma_v^2 E[B_j] \end{aligned} \tag{B.22}$$

$$T_{ij}^{42} = H_j^* E|V_i(m)|^2 S_j^*(m')V_j(m')] = 0 \tag{B.23}$$

$$T_{ij}^{43} = H_j E[|V_i(m)|^2 S_j(m')V_j^*(m')] = 0 \tag{B.24}$$

$$\begin{aligned} T_{ij}^{44} &= E[|V_i(m)|^2|V_j(m')|^2] \\ &= E[V_i(m)V_i^*(m)V_j(m')V_j^*(m')] \\ &= E[V_i(m)V_i^*(m)]E[V_j(m')V_j^*(m')] + E[V_i(m)V_j^*(m')]E[V_i^*(m)V_j(m')] \\ &= \sigma_v^4(1 + \delta_{ij}\delta_{mm'}) \end{aligned} \tag{B.25}$$

The above derivation makes use of a standard formula for the 4th moment of jointly Gaussian complex circular random variables [32], [33]. The following was used to compute joint moments of $S_i(m)$ and $S_j(m')$:

$$\begin{aligned} &E[S_i(m)S_i^*(m)S_j(m')S_j^*(m')] \\ &\qquad = \sum_{b_0=0}^{1} \cdots \sum_{b_{K-1}=0}^{1} E[S_i(m)S_i^*(m)S_j(m')S_j^*(m')\big|\boldsymbol{B} = \boldsymbol{b}] \Pr(\boldsymbol{B} = \boldsymbol{b}) \\ &\qquad = \sum_{b_0=0}^{1} \cdots \sum_{b_{K-1}=0}^{1} b_i b_j(1 + \delta_{ij}\delta_{mm'}) \Pr(\boldsymbol{B} = \boldsymbol{b}) \\ &\qquad = E[B_i B_j](1 + \delta_{ij}\delta_{mm'}) \end{aligned} \tag{B.26}$$

since:

$$\begin{aligned} E[S_i(m)S_i^*(m)S_j(m')S_j^*(m')\big|\boldsymbol{B} = \boldsymbol{b}] &= E[|S_i(m)|^2\big|\boldsymbol{B} = \boldsymbol{b}]E[|S_j(m')|^2\big|\boldsymbol{B} = \boldsymbol{b}] \\ &\quad + E[S_i(m)S_j^*(m')\big|\boldsymbol{B} = \boldsymbol{b}]E[S_i^*(m)S_j(m')\big|\boldsymbol{B} = \boldsymbol{b}] \\ &= b_i b_j(1 + \delta_{ij}\delta_{mm'}) \end{aligned} \tag{B.27}$$

$$
\begin{aligned}
\therefore E[\tilde{Y}_i\tilde{Y}_j] \\
&= E[Y_iY_j] - E[Y_i]E[Y_j] \\
&= M^2G_iG_jE[B_iB_j] + MG_i^2E[B_i]\delta_{ij} + M^2\sigma_v^4 + M\sigma_v^4\delta_{ij} \\
&\quad + M^2G_i\sigma_v^2E[B_i] + M^2G_j\sigma_v^2E[B_j] + MG_i\sigma_v^2E[B_i]\delta_{ij} + MG_i\sigma_v^2E[B_i]\delta_{ij} \\
&\quad - M^2\big(E[B_i]G_i + \sigma_v^2\big)\big(E[B_j]G_j + \sigma_v^2\big) \\
&= M^2G_iG_j\big(E[B_iB_j] - E[B_i]E[B_j]\big) + M\delta_{ij}\big(G_i^2E[B_i] + 2G_i\sigma_v^2E[B_i] + \sigma_v^4\big) \qquad \text{(B.28)}
\end{aligned}
$$

Bibliography

[1] A. Ghasemi and E. S. Sousa, "Spectrum sensing in cognitive radio networks: requirements, challenges and design trade-offs," *IEEE Communications Magazine*, vol. 46, no. 4, pp. 32–39, Apr. 2008.

[2] C. da Silva, B. Choi, and K. Kim, "Distributed spectrum sensing for cognitive radio systems," in *Proc. Information Theory and Applications Workshop*, Jan. 2007, pp. 120–123.

[3] S. Haykin, "Cognitive radio: brain-empowered wireless communications," *IEEE J. Sel. Areas in Communication*, vol. 23, no. 2, pp. 201–220, Feb. 2005.

[4] T. Yücek and H. Arslan, "A survey of spectrum sensing algorithms for cognitive radio applications," *IEEE Communications Surveys & Tutorials*, vol. 11, no. 1, pp. 116–130, Mar. 2009.

[5] C. Cordeiro, K. Challapali, D. Birru, and S. Shankar, "IEEE 802.22: An introduction to the first wireless standard based on cognitive radios," in *J. of Communications*, vol. 25, no. 1, Apr. 2006, pp. 38–47.

[6] J. G. Proakis and M. Salehi, *Digital Communications*, 5th ed. McGraw Hill, 2008.

[7] Z. Quan, S. Cui, H. V. Poor, and A. H. Sayed, "Collaborative wideband sensing for cognitive radios," *IEEE Signal Processing Magazine*, vol. 25, no. 6, pp. 60–73, Nov. 2008.

[8] K. Kim, I. A. Akbar, K. K. Bae, J. Um, C. M. Spooner., and J. H. Reed, "Cyclostationary approaches to signal detection and classification in cognitive radio," in *Proc. IEEE Int. Symp. New Frontiers in Dynamic Spectrum Access Networks*, Apr. 2007, pp. 212–215.

[9] Z. Tian and G. B. Giannakis, "A wavelet approach to wideband spectrum sensing for cognitive radios," in *Proc. Int. Conf. Cognitive Radio Oriented Wireless Networks and Communications*, Jun. 2006, pp. 1–5.

[10] A. Ghasemi and E. Sousa, "Collaborative spectrum sensing for opportunistic access in fading environments," in *Proc. IEEE Int. Symp. New Frontiers in Dynamic Spectrum Access Networks*, Nov. 2005, pp. 131–136.

[11] R. Chen, J.-M. Park, and K. Bian, "Robust distributed spectrum sensing in cognitive radio networks," in *Proc. 27th Conf. Computer Communications (INFOCOM)*, Apr. 2008, pp. 1876–1884.

[12] Z. Quan, S. Cui, A. H. Sayed, and H. V. Poor, "Optimal multiband joint detection for spectrum sensing in cognitive radio networks," *IEEE Trans. Signal Processing*, vol. 57, no. 3, pp. 1128–1140, Mar. 2009.

[13] Z. Quan, S. Cui, and A. H. Sayed, "Optimal linear cooperation for spectrum sensing in cognitive radio networks," *IEEE J. Sel. Topics in Signal Processing*, vol. 2, no. 1, pp. 28–40, Feb. 2008.

[14] J. A. Bazerque and G. B. Giannakis, "Distributed spectrum sensing for cognitive radio networks by exploiting sparsity," *IEEE Trans. Signal Processing*, vol. 58, no. 3, pp. 1847–1862, Mar. 2010.

[15] B.-J. Kang, "Spectrum sensing issues in cognitive radio networks," in *Int. Symp. Communications and Information Technology*, Jan. 2009, pp. 824–828.

[16] C.-H. Hwang, G.-L. Lai, and S.-C. Chen, "Spectrum sensing in wideband OFDM cognitive radios," *IEEE Trans. Signal Processing*, vol. 58, no. 2, pp. 709–719, Feb. 2010.

[17] Z. Tian and G. B. Giannakis, "Compressed sensing for wideband cognitive radios," in *Int. Conf. Acoustics, Speech, Signal Processing*, vol. 4, Apr. 2007, pp. 1357–1360.

[18] S. Mallat and W. Hwang, "Singularity detection and processing with wavelets," *IEEE Trans. Information Theory*, vol. 38, no. 2, pp. 617–643, Mar. 1992.

[19] Z. Cvetkovic and M. Vetterli, "Discrete-time wavelet extrema representation: design and consistent reconstruction," *IEEE Trans. Signal Processing*, vol. 43, no. 3, pp. 681–693, Mar. 1995.

[20] N. Khambekar, L. Dong, and V. Chaudhary, "Utilizing ofdm guard interval for spectrum sensing," in *Proc. IEEE Wireless Communications and Networking Conf.*, Mar. 2007, pp. 38–42.

[21] M. Oner and F. Jondral, "Cyclostationarity based air interface recognition for software radio systems," in *Proc. IEEE Radio and Wireless Conf.*, Sep. 2004, pp. 263–266.

[22] W. Gardner, "Measurement of spectral correlation," *IEEE Trans. Acoustics, Speech and Signal Processing*, vol. 34, no. 5, pp. 1111–1123, Oct. 1986.

[23] W. A. Gardner and C. M. Spooner, "Signal interception: performance advantages of cyclic-feature detectors," *IEEE Trans. Communications*, vol. 40, no. 1, pp. 149–159, Jan. 1992.

[24] N. C. Jones and P. A. Pevzner, *An Introduction to Bioinformations Algorithms*, 1st ed. MIT Pres, 2004.

[25] R. Tandra and A. Sahai, "SNR walls for signal detection," *IEEE J. Sel. Topics in Signal Processing*, vol. 2, no. 1, pp. 4–17, Feb. 2008.

[26] D. Cabric, S. M. Mishra, and R. W. Brodersen, "Implementation issues in spectrum sensing for cognitive radios," in *Proc. Asilomar Conf. Signals, Systems and Computers*, Nov. 2004, pp. 772–776.

[27] H. V. Poor, *An Introduction to Signal Detection and Estimation*, 2nd ed. Springer-Verlag, 1994.

[28] J. G. Proakis and D. K. Manolakis, *Digital Signal Processing*, 4th ed. Prentice Hall, 2006.

[29] A. Goldsmith, *Wireless Communications*. Cambridge University Press, 2006.

[30] A. Papoulis, *Probability, Random Variables, and Stochastic Processes*, 2nd ed. McGraw Hill, 1984.

[31] E. Visotsky, S. Kuffner, and R. Peterson, "On collaborative detection of tv transmissions in support of dynamic spectrum sharing," in *Proc. IEEE Int. Symp. New Frontiers in Dynamic Spectrum Access Networks*, Nov. 2005, pp. 338–345.

[32] R. A. Monzingo and T. Miller, *Introduction to Adaptive Arrays*. SciTech Publishing, 2004.

[33] I. S. Reed, "On a moment theorem for complex gaussian processes," *IRE Trans. Information Theory*, vol. 8, no. 3, pp. 194 – 195, May 1962.